Contents lists available at ScienceDirect

Journal of Non-Newtonian Fluid Mechanics

journal homepage: www.elsevier.com/locate/jnnfm

Linear instability of viscoelastic interfacial Hele-Shaw flows: A Newtonian fluid displacing an UCM fluid

Zhiying Hai, Prabir Daripa *

Department of Mathematics, Texas A&M University, 155 Ireland St, College Station, 77840, TX, USA

ARTICLE INFO

Keywords:
Saffman–Taylor instability
Viscous fingering
Hele-Shaw flow
Linear stability
Upper convected Maxwell fluid
Elasticity

ABSTRACT

We theoretically study the linear stability of the Saffman–Taylor problem where a viscous Newtonian fluid (with viscosity η^l) displaces an Upper Convected Maxwell (UCM) fluid (with viscosity η^r) in a rectilinear Hele-Shaw cell. The dispersion relation is given by the roots of a cubic polynomial with coefficients depending on wavenumber along with several dimensionless groups as parameters. Using Routh–Hurwitz stability criterion, we show that the viscosity ratio η^r/η^l still plays a decisive role in determining stability (stable if $\eta^r/\eta^l \leq 1$). If $\eta^r/\eta^l > 1$, the flow is more unstable than an identical Newtonian–Newtonian setup and the most unstable wavenumber is larger. Increasing Deborah number, capillary number or flow speed worsens the instability. Elasticity has a variety of effects and can give rise up to three types of singular behaviors: (i) there exists infinitely many distinct wavenumbers at which the velocity becomes singular, (ii) stress becomes singular when the wavenumber exceeds a certain value; and (iii) a resonance phenomenon occurs when η^r/η^l is large, where the growth rate increases very rapidly near certain wavenumber and eventually becomes singular when the displacing fluid is inviscid.

1. Introduction

Interfacial flows are ubiquitous in nature and play very important roles in many areas of science and technology. Over the last few decades, there have been significant advances in the theory and modeling of such flows because of their relevance to environment, industry, and fundamental science. One of the simplest of interfacial flows is Hele-Shaw flows which refer to flows in a Hele-Shaw cell. A Hele-Shaw cell is a device consisting of two closely spaced parallel plates so that the distance between the plates is very small compared to the dimensions of the plates. Displacement of a viscous fluid by a less viscous one in a Hele-Shaw cell has received considerable attention because of ease in performing experiments involving such displacement processes and its connection to porous media flows.

For Hele-Shaw flows involving single Newtonian fluid, exact calculation shows that the average velocity between two plates is analogous to the Darcy's law for flows of a Newtonian fluid in a homogeneous porous medium. Since the fifties, this analogy has been the driving force behind considerable research in Hele-Shaw flows in which a viscous fluid displaces another viscous fluid, usually more viscous as it happens in secondary and enhanced stages of oil recovery. When the displaced fluid is more viscous, the interface becomes unstable and develops into finger-like patterns as time progresses. This instability of the interface is commonly referred to as viscous fingering or Saffman–Taylor (ST) instability [1] even though a similar calculation that included the effect of surface tension was carried out about the same time by Chouke et al. [2]. However, first calculation of this interfacial instability was done even earlier by Hill [3] and hence, as suggested by Homsy [4], this instability should perhaps be called the "Hill Instability".

The analysis of this fingering instability for immiscible displacements requires, in addition to the field equations in the two fluid regions, the location of the interface and interfacial conditions. The original two-dimensional analysis of linear stability for this fingering instability is performed in the plane of the plates with the equations that have been depth-averaged by averaging across the gap between the plates. The interface conditions, namely kinematic and dynamic conditions, are also pre-averaged (see Homsy [4] and Reinelt [5]). There are delicate issues in all of this which have been discussed in the review articles of Homsy [4] and Saffman [6].

The interface conditions used in Saffman and Taylor [1] have been refined in Park & Homsy [7] leading to the conclusion that they were in reasonable agreement for small capillary numbers. The stability analysis gives many pertinent information including stability criterion or equivalently marginal curve separating the stable and unstable regions in the parameter space of the problem. This stability criterion can also be obtained with ad-hoc calculation based on consideration of

* Corresponding author.
E-mail address: daripa@tamu.edu (P. Daripa).

https://doi.org/10.1016/j.jnnfm.2022.104773
Received 9 September 2021; Received in revised form 12 January 2022; Accepted 17 February 2022

competing capillary and viscous forces as shown in Homsy [4]. When the conditions are unfavorable, the interface topology develops into myriad of fingers as time progresses. There is considerable work on the number, shape and speed of these fingers including the speed of the solitary finger in the large time limit.

Above deliberation is exclusively for immiscible displacement processes in a Hele-Shaw cell involving Newtonian fluids. Investigation in similar processes involving non-Newtonian fluids such as liquid crystals, polymer solutions, melts, and colloidal fluids started in the eighties where strikingly different fingering patterns [8–15] are observed. Non-Newtonian fluids can show one or more of the following properties: shear dependent viscosity, elasticity and yield stress among many others. Depending on the extent to which these properties affect the flow, the fingering patterns can show a range of complexity from finger formation of various widths to complex patterns of fractal type. The effects of different non-Newtonian properties can often compete against each other, for example shear thinning property usually leads to narrower finger as opposed to elastic effect which usually tends to widen the finger width [16].

Understanding and disentangling the effects of different non-Newtonian properties on the overall dynamics of instabilities is extremely challenging. Despite extensive efforts [17–20,20–32], the subject is still much less developed in comparison to the Newtonian counterparts, especially on the role of elasticity. The first theoretical attempt on such matter was made by Wilson [20] who considered air displacing an Oldroyd-B fluid [33] or an UCM fluid and studied the linear stability in the regime of moderate to high Deborah number. The author considered the air to be inviscid which in the Stokes' regime is simply a fluid of constant pressure. Since the averaging procedure used in Newtonian case is no longer valid on the non-Newtonian side due to the nonlinearity in the constitutive relations, Wilson started with the full set of equations from which a system of linearized perturbation equations were then obtained in the thin gap limit. Using a normal mode ansatz for the perturbations, the equations were then solved numerically to obtain the dispersion relations. A sharp increase, although remain finite, in the growth rate as Deborah number increases is predicted which the author ascribed to a resonance phenomenon.

More than two decades later, Mora and Manna [32] considered the same problem (air displacing UCM) using a semi-analytical approach. They also obtained disturbances with large growth rate and predicted that the growth rate can eventually become singular when a certain parameter exceeds a critical value. They also performed experiments and observed fracturing, thus establishing the connection of the resonance phenomenon to something observable in experiments. About the same time, Daripa et al. [34,35] considered the same problem after dropping the time derivative terms in the constitutive relation for an Oldroyd-B fluid. There is no rigorous physical or mathematical justification for this simplification except to make the problem analytically tractable. This subsequently led to an explicit formula for the dispersion relation. This dispersion relation also shows the existence of singular disturbances with large growth rates in spite of gross simplification of the underlying modeling equations.

This paper aims to provide additional insight on the role of elasticity in causing fingering instabilities and studies the linear stability of the two-phase Hele-Shaw flow where a viscous Newtonian fluid displaces an UCM fluid in the regime of moderate to high Deborah number. The solution technique is analytical and produces the dispersion relation in closed form and recovers results obtained by Saffman & Taylor [1], Wilson [20] and Mora & Manna [32] as special cases.

The paper is organized as follows. In Section 2, the setup is described and the governing equations are presented. In Section 3, the equations are non-dimensionalized and a set of reduced equations are obtained in the thin gap limit while keeping the elastic effect to the leading order. In Section 4, the equations are perturbed and linearized about a basic flow of the form $\boldsymbol{u}_0 = (U(y), 0, 0)$. The method of normal mode is applied to the linearized equations, which then leads to an inhomogeneous boundary value problem (BVP) with variable coefficients. In Section 5, the BVP is solved analytically where the solution involves weighted integral of Bessel functions of first kind of order $-1/4$ and $1/4$. In Section 6, the solution of BVP is then inserted into the interface conditions to obtain the dispersion relation $\mathcal{F} = 0$, where $\mathcal{F}$ is a cubic polynomial in growth rate with coefficients depending on the wavenumber, capillary number, Deborah number, flow speed and viscosity ratio of the two fluids. The detailed analysis on the roots is given. Further, $\mathcal{F}$ reduces to a linear polynomial in the limit of small relaxation time and the classical ST result is recovered. The special case of air displacing UCM fluid is also considered where $\mathcal{F}$ becomes quadratic, and comparisons with previous works by Wilson [20] and Mora and Manna [32] are made. Finally, conclusions are made in Section 7.

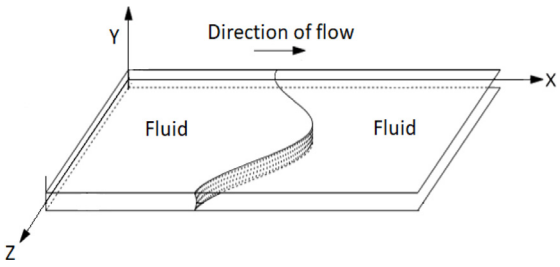

Fig. 1. A section of the rectilinear Hele-Shaw flow.

2. Setup description and governing equations

Two fluids are confined in a rectilinear Hele-Shaw cell with a gap width $2b$ and moving to the $+x$ direction due to a driving source located upstream ($-x$ direction). A section of the setup is shown in Fig. 1. The fluids are assumed to be immiscible, incompressible and homogeneous. The interface that separates the two fluids has constant interfacial tension γ. The thin film effect and y direction variation of the interface are neglected [36]. We further assume that the interface can be the described an equation of the form $x = \zeta(z,t)$. The displacing fluid occupying $x < \zeta(z,t)$ is Newtonian whereas the displaced fluid occupying $\zeta(z,t) < x$ is UCM. Throughout the development, inertial terms and gravity effect are neglected. The governing equations are given by Eqs. (1)–(4) below, where superscript 'l' or 'r' refers to the quantity is restricted to the Newtonian or UCM layer respectively.

$$\left.\begin{aligned} \nabla\cdot\boldsymbol{u}^l = 0, \quad \nabla p^l = \eta^l \Delta \boldsymbol{u}^l, \\ \nabla\cdot\boldsymbol{u}^r = 0, \quad \nabla p^r = \nabla\cdot\boldsymbol{\tau}, \\ \boldsymbol{\tau} + \lambda\tfrac{D_1\boldsymbol{\tau}}{Dt} = \eta^r(\nabla\boldsymbol{u}^r + (\nabla\boldsymbol{u}^r)^T). \end{aligned}\right\} \tag{1}$$

The symbol $\boldsymbol{u} = (u, v, w)$ represents the velocity field where u, v, w are the components in x, y, and z directions respectively, p is the pressure, $\nabla = (\partial_x, \partial_y, \partial_z)$, $\Delta = \nabla\cdot\nabla$, η and λ are viscosity and relaxation time respectively. D_1/Dt is the upper convected time derivative. Non-slip and non-penetration conditions at the cell walls are

$$\boldsymbol{u}^l = \boldsymbol{u}^r = 0, \quad \text{at } y = \pm b \tag{2}$$

At the interface $x = \zeta(z,t)$, we impose gap averaged kinematic and dynamic conditions. The former states the interface velocity is same as the gap averaged fluid velocity on the two sides

$$\zeta_t = \langle u^r\rangle - \langle w^r\rangle\zeta_z = \langle u^l\rangle - \langle w^l\rangle\zeta_z, \tag{3}$$

where $\langle\cdot\rangle$ represents the average across the gap. The dynamic condition states that the discontinuity of the average normal stress is balanced by the interfacial tension $-(\langle p^r\rangle-\langle p^l\rangle)+\boldsymbol{n}\cdot(\langle\boldsymbol{\tau}\rangle-\eta^l\langle\nabla\boldsymbol{u}^l+(\nabla\boldsymbol{u}^l)^T\rangle)\boldsymbol{n}=\gamma\nabla\cdot\boldsymbol{n}$, where $\boldsymbol{n}$ is the unit normal of the interface pointing into the UCM fluid. Equivalently, this is rewritten as

$$\begin{aligned}&(1+\zeta_z^2)(\langle p^r\rangle-\langle p^l\rangle)-\left(\langle\tau^{xx}\rangle-2\langle\tau^{xz}\rangle\zeta_z+\langle\tau^{zz}\rangle\zeta_z^2\right)+\cdots\\&2\eta^l\left(\langle u_x^l\rangle-\langle u_z^l+w_x^l\rangle\zeta_z+\langle w_z^l\rangle\zeta_z^2\right)=\frac{\gamma\zeta_{zz}}{(1+\zeta_z^2)^{1/2}}.\end{aligned}\tag{4}$$

3. Model equations in the thin gap limit

Due to the Hele-Shaw geometry, certain terms from (1)–(4) can be dropped in the thin gap limit. To do so, a set of scales must be properly chosen first. Away from the interface, the dominant part of the flow field is parallel to the cell plates, therefore the relative sizes of physical variables can be captured by studying flow of the form $\boldsymbol{u}=(u(y),0,0)$ for which (1) reduces to

$$\left.\begin{aligned}&p_x^l=\eta^l u_{yy}^l,\quad p_y^l=0,\quad p_z^l=0,\\&p_x^r=\eta^r u_{yy}^r,\quad p_y^r=0,\quad p_z^r=0,\\&\tau^{xy}=\tau^{yx}=\eta^r u_y^r,\quad \tau^{xx}=2\lambda u_y^r\tau^{xy},\end{aligned}\right\}\tag{5}$$

where all other components of $\boldsymbol{\tau}$ are zero. Let L and V be the characteristic length and velocity scales in the lateral direction, b be the length scale in the transverse direction, and G a characteristic pressure.

$$\left.\begin{aligned}&(x,y,z)\propto(L,b,L),\quad (u,v,w)\propto(V,Vb/L,V),\\&t\propto L/V,\quad p\propto G.\end{aligned}\right\}\tag{6}$$

Define the following

$$\overline{\eta}=\eta^l+\eta^r,\quad R_\eta^l=\eta^l/\overline{\eta},\quad R_\eta^r=\eta^r/\overline{\eta}.\tag{7}$$

The use of $\overline{\eta}$ is to have a consistent set of units for both fluid layers. The difference between η^l and η^r is reflected in $R_\eta^{l,r}$ and will be carried into the scaled equations. Inserting (6) and (7) into (5), together with symmetry of $\boldsymbol{\tau}$, we have the following scales

$$\tau^{xy},\tau^{yz}\propto\overline{\eta}V/b,\quad \tau^{xx},\tau^{xz},\tau^{zz}\propto\lambda\overline{\eta}V^2/b^2,\quad \tau^{yy}\propto\overline{\eta}V/L,$$

and the following relation by balancing the unit

$$V=\epsilon^2GL/\overline{\eta}.\tag{8}$$

Using above scaling scheme, the non-dimensionalized version of Eqs. (1)–(4) contain the following dimensionless groups

$$\epsilon=b/L,\quad De=\epsilon^2G\lambda/\overline{\eta},\quad Ca=GL/\gamma,\tag{9}$$

where ϵ is the characteristic aspect ratio of the Hele-Shaw cell, De is the Deborah number, and Ca is the capillary number. In the thin gap limit $\epsilon\to0$, elastic behavior of the UCM layer is apparent if $De\sim\mathcal{O}(1)$ or larger. Since the characteristic pressure G is ultimately determined by the external driving source, it can be taken as an adjustable parameter to achieve this, for example, $De\sim\mathcal{O}(1)$ if $G\sim\mathcal{O}(\epsilon^{-2})$. In such regime, the non-dimensionalized equations obtained from (1)–(4) at the leading order are given by (10)–(14) below,

$$\left.\begin{aligned}&u_x^l+v_y^l+w_z^l=0,\quad p_y^l=0,\\&p_x^l=R_\eta^l u_{yy}^l,\quad p_z^l=R_\eta^l w_{yy}^l.\end{aligned}\right\}\tag{10}$$

$$\left.\begin{aligned}&u_x^r+v_y^r+w_z^r=0,\qquad p_y^r=0,\\&p_x^r=R_\eta^r(De(\tau_x^{xx}+\tau_z^{xz})+\tau_y^{xy}),\\&p_z^r=R_\eta^r(De(\tau_x^{xz}+\tau_z^{zz})+\tau_y^{yz}),\\&L\tau^{xy}=u_y^r+De^2(v_x^r\tau^{xx}+v_z^r\tau^{xz})\cdots\\&+De((u_x^r+v_y^r)\tau^{xy}+u_z^r\tau^{yz}+u_y^r\tau^{yy}),\\&L\tau^{yz}=w_y^r+De^2(v_x^r\tau^{xz}+v_z^r\tau^{zz})\cdots\\&+De((w_z^r+v_y^r)\tau^{yz}+w_x^r\tau^{xy}+w_y^r\tau^{yy}),\\&L\tau^{xz}=(u_y^r\tau^{yz}+w_y^r\tau^{xy})\cdots\\&+De((u_x^r+w_z^r)\tau^{xz}+u_z^r\tau^{zz}+w_x^r\tau^{xx}),\\&L\tau^{xx}=2(u_y^r\tau^{xy}+De(u_x^r\tau^{xx}+u_z^r\tau^{xz})),\\&L\tau^{yy}=2(v_y^r+De(v_x^r\tau^{xy}+v_y^r\tau^{yy}+v_z^r\tau^{yz})),\\&L\tau^{zz}=2(w_y^r\tau^{yz}+De(w_z^r\tau^{zz}+w_x^r\tau^{xz})).\end{aligned}\right\}\tag{11}$$

where

$$L=I+De\left(\partial_t+u^r\partial_x+v^r\partial_y+w^r\partial_z\right)\tag{12}$$

At the cell plates $y=\pm1$

$$u^l=v^l=w^l=u^r=v^r=w^r=0.\tag{13}$$

At the interface $x=\zeta(z,t)$

$$\left.\begin{aligned}&\zeta_t=\langle u^r\rangle-\langle w^r\rangle\zeta_z,\\&\langle u^r\rangle-\langle w^r\rangle\zeta_z=\langle u^l\rangle-\langle w^l\rangle\zeta_z,\\&(1+\zeta_z^2)(p^r-p^l)-\cdots\\&R_\eta^r De(\langle\tau^{xx}\rangle-2\langle\tau^{xz}\rangle\zeta_z+\langle\tau^{zz}\rangle\zeta_z^2)=\frac{Ca^{-1}\zeta_{zz}}{(1+\zeta_z^2)^{\frac{1}{2}}}.\end{aligned}\right\}\tag{14}$$

4. Linear stability

Now we consider the linear stability of the basic flow $\boldsymbol{u}_0=(U(y),0,0)$ for Eqs. (10)–(14). The basic solution satisfying $U=0$ at $y=\pm1$ is easily found to be

$$\left.\begin{aligned}&U^l=-3\langle U^l\rangle(y^2-1)/2,\quad \langle U^l\rangle=-p_{0,x}^l/(3R_\eta^l),\\&U^r=-3\langle U^r\rangle(y^2-1)/2,\quad \langle U^r\rangle=-p_{0,x}^r/(3R_\eta^r),\\&\tau_0^{xy}=U_y^r,\quad \tau_0^{xx}=2U_y^r\tau_0^{xy}\end{aligned}\right\}\tag{15}$$

where all other stress components are zero and $p_{0,x}^l$, $p_{0,x}^r$ are negative constants. Interface conditions (14) give

$$\zeta_0=\langle U^r\rangle t,\quad \langle U^r\rangle=\langle U^l\rangle,\quad p_0^r-p_0^l=R_\eta^r De\langle\tau_0^{xx}\rangle.\tag{16}$$

By definition of $\langle U^l\rangle$ and $\langle U^r\rangle$ given in $(15)_2$ and $(15)_4$, $(16)_2$ implies

$$p_{0,x}^r-p_{0,x}^l=-3\langle U^r\rangle(R_\eta^r-R_\eta^l)\tag{17}$$

By $(16)_2$, we may drop the superscript r and l on $\langle U^l\rangle$ and $\langle U^r\rangle$ from now on. The linearized (10)–(14) about the basic solution (15) and (16) can be easily obtained. On the resulting equations, the moving frame of reference $x\mapsto x-\langle U\rangle t$ is used, and the following normal mode ansatz is assumed

$$\left.\begin{aligned}&(u^l,w^l,p^l)=\left(\hat{u}^l,\hat{w}^l,\hat{p}^l\right)e^{\mu t+ikz},\\&(u^r,w^r,p^r,\tau^{ij})=\left(\hat{u}^r,\hat{w}^r,\hat{p}^r,\hat{\tau}^{ij}\right)e^{\mu t+ikz},\\&\zeta=\hat{\zeta}e^{\mu t+ikz},\end{aligned}\right\}\tag{18}$$

where the quantities with hat are complex valued amplitudes depending on x and y but not t. μ is the temporal growth rate of perturbations, potentially complex valued.

The resulting interface conditions in (14) become

$$\left.\begin{aligned}&\mu\hat{\zeta}=\langle\hat{u}^r\rangle,\quad \langle\hat{u}^r\rangle=\langle\hat{u}^l\rangle,\\&\hat{p}^r-\hat{p}^l-R_\eta^r De\langle\hat{\tau}^{xx}\rangle\cdots\\&=\left(-k^2Ca^{-1}+3\langle U\rangle(R_\eta^r-R_\eta^l)\right)\hat{\zeta}\end{aligned}\right\}\quad\text{at } x=0\tag{19}$$

where (17) is used to obtain the second term on the right hand side of Eq. $(19)_3$. Inserting $(18)_1$ into (10) gives

$$\left.\begin{aligned} \hat{u}^l_x + \hat{v}^l_y + ik\hat{w}^l = 0, \\ \hat{p}^l_y = 0, \quad \hat{p}^l_x = R^l_\eta \hat{u}^l_{yy}, \quad ik\hat{p}^l = R^l_\eta \hat{w}^l_{yy}. \end{aligned}\right\} \tag{20}$$

Since $(20)_2$–$(20)_4$ imply $\hat{u}^l$, $\hat{w}^l$ are quadratic in y, v^l must be either cubic in y or identically 0 by $(20)_1$. The former is not possible because non-slip condition implies both v^l_y and v^l must vanish at $y = \pm 1$. In turn, $(20)_1$, $(20)_3$ and $(20)_4$ imply $\hat{p}^l_{xx} - k^2\hat{p}^l = 0$, the solution of which, subject to $\hat{p}^l \to 0$ as $x \to -\infty$, is given by

$$\hat{p}^l = \hat{p}^- e^{|k|x}, \tag{21}$$

for some constant $\hat{p}^-$. From above and $(20)_3$, $\hat{u}^l$ can be easily found. Taking average over $y \in (-1, 1)$ yields

$$\langle \hat{u}^l \rangle = -|k|\hat{p}^- e^{|k|x}/(3R^l_\eta). \tag{22}$$

For the UCM layer, it is physically plausible to assume a two dimensional disturbance on the velocity field, i.e. $v^r = 0$, because the fluid is confined in a very thin gap. As a result, equations in (11) after linearization are given by

$$\left.\begin{aligned} \hat{u}^r_x + ik\hat{w}^r = 0, \qquad \hat{p}^r_y = 0, \\ \hat{p}^r_x = R^r_\eta \left(De(\hat{\tau}^{xx}_x + ik\hat{\tau}^{xz}) + \hat{\tau}^{xy}_y\right), \\ ik\hat{p}^r = R^r_\eta \left(De(\hat{\tau}^{xz}_x + ik\hat{\tau}^{zz}) + \hat{\tau}^{yz}_y\right), \\ L\hat{\tau}^{xy} = \hat{u}^r_y + DeV^*_y \hat{u}^r_x + DeV^*_y \hat{\tau}^{yy}, \\ L\hat{\tau}^{yz} = \hat{w}^r_y + DeV^*_y \hat{w}^r_x, \\ L\hat{\tau}^{xx} = 2V^*_y \left(\hat{\tau}^{xy} + \hat{u}_y + 2DeV^*_y \hat{u}^r_x\right), \\ L\hat{\tau}^{xz} = V^*_y(\hat{\tau}^{yz} + \hat{w}^r_y + 2DeV^*_y \hat{w}^r_x), \\ L\hat{\tau}^{yy} = L\hat{\tau}^{zz} = 0, \end{aligned}\right\} \tag{23}$$

where (the letter L is reused and not to be confused with (12))

$$\left.\begin{aligned} L = (1 + \mu De)I + DeV^*\partial_x, \\ V^* = -3\langle U \rangle (y^2 - 1/3)/2. \end{aligned}\right\} \tag{24}$$

Notice the solutions for $(23)_9$ and $(23)_{10}$ are proportional to $exp(-(1 + \mu De)x/(DeV^*))$. Since V^* changes sign at $y = \pm 1/\sqrt{3}$, it must be $\hat{\tau}^{yy} = \hat{\tau}^{zz} = 0$ to be continuous. In turn, (23) reads

$$\left.\begin{aligned} \hat{u}^r_x + ik\hat{w}^r = 0, \qquad \hat{p}^r_y = 0, \\ \hat{p}^r_x = R^r_\eta \left(De(\hat{\tau}^{xx}_x + ik\hat{\tau}^{xz}) + \hat{\tau}^{xy}_y\right), \\ ik\hat{p}^r = R^r_\eta \left(De\hat{\tau}^{xz}_x + \hat{\tau}^{yz}_y\right), \\ L\hat{\tau}^{xy} = \hat{u}^r_y + DeV^*_y \hat{u}^r_x, \quad L\hat{\tau}^{yz} = \hat{w}^r_y + DeV^*_y \hat{w}^r_x, \\ L\hat{\tau}^{xx} = 2V^*_y \left(\hat{\tau}^{xy} + \hat{u}_y + 2DeV^*_y \hat{u}^r_x\right), \\ L\hat{\tau}^{xz} = V^*_y(\hat{\tau}^{yz} + \hat{w}^r_y + 2DeV^*_y \hat{w}^r_x). \end{aligned}\right\} \tag{25}$$

Further, $(25)_1$ imply $L[\hat{\tau}^{xy}_x + ik\hat{\tau}^{yz}] = 0$ and $L[\hat{\tau}^{xx}_x + 2ik\hat{\tau}^{xz}] = 2V^*_y \left(\hat{\tau}^{xy}_x + ik\hat{\tau}^{yz}\right)$. For the solutions to be continuous, it must be

$$\hat{\tau}^{xy}_x + ik\hat{\tau}^{yz} = 0, \qquad \hat{\tau}^{xx}_x + 2ik\hat{\tau}^{xz} = 0. \tag{26}$$

Differentiating $(25)_3$ w.r.t to x and multiplying $(25)_4$ by ik, then adding the two equations give $\hat{p}^r_{xx} - k^2\hat{p}^r = 0$. As a result, the solution subject to $\hat{p}^r \to 0$ as $x \to \infty$ is given by

$$\hat{p}^r = \hat{p}^+ e^{-|k|x}, \tag{27}$$

for some constant $\hat{p}^+$. Applying the operator L to $(25)_3$

$$\begin{aligned} &L\hat{p}_x/R^r_\eta = DeL[\hat{\tau}^{xx}_x + ik\hat{\tau}^{xz}] + L\hat{\tau}^{xy}_y \\ &= -ikDeL\hat{\tau}^{xz} + [L\hat{\tau}^{xy}]_y - DeV^*_y \hat{\tau}^{xy}_x \\ &= -ikDeV^*_y(\hat{w}^r_y + 2DeV^*_y \hat{w}^r_x) + [\hat{u}^r_y + DeV^*_y \hat{u}^r_x]_y \\ &= DeV^*_y[\hat{u}^r_y + 2DeV^*_y \hat{u}^r_x]_x + [\hat{u}^r_y + DeV^*_y \hat{u}^r_x]_y. \end{aligned} \tag{28}$$

In the second equality above, $(26)_2$ is used along with the definition of L. $(25)_5$, $(25)_8$ and $(26)_1$ are used to obtain the third equality, and $(25)_1$ for the fourth.

5. Boundary value problem

By (27) and $(24)_2$, (28) reads

$$\hat{\mathcal{L}}\hat{u} = (-|k|\hat{p}^+/R^r_\eta)(1 + \mu De - \hat{k}/3 + \hat{k}y^2)e^{-|k|x}, \tag{29}$$

where

$$\left.\begin{aligned} \hat{\mathcal{L}} = \frac{\partial^2}{\partial y^2} + 4\omega y \frac{\partial^2}{\partial y \partial x} + 2\omega \frac{\partial}{\partial x} + 8\omega^2 y^2 \frac{\partial^2}{\partial x^2}, \\ \hat{k} = -\omega|k|, \quad \omega = -3\langle U \rangle De/2 \end{aligned}\right\} \tag{30}$$

Eq. (29) needs to be solved subject to $\hat{u} = 0$ at $y = \pm 1$ with far field condition $\hat{u} \to 0$ as $x \to \infty$. In Appendix A.3, it is shown that $\hat{u}$ must take on the following form so that the solution is unique

$$\hat{u}^r = (-|k|\hat{p}^+/R^r_\eta)\tilde{u}(y)e^{-|k|x}. \tag{31}$$

Substituting (31) into (29) gives

$$\mathcal{L}\tilde{u} = \psi \tag{32}$$

where

$$\left.\begin{aligned} \mathcal{L} = \frac{d^2}{dy^2} + 4\hat{k}y\frac{d}{dy} + (8\hat{k}^2y^2 + 2\hat{k})I, \\ \psi(y) = 1 + \mu De - \hat{k}/3 + \hat{k}y^2. \end{aligned}\right\} \tag{33}$$

Substituting $\tilde{u} = exp(-\hat{k}y^2)\breve{u}$ in $\mathcal{L}\tilde{u} = 0$ gives

$$\breve{u}_{yy} + 4\hat{k}^2y^2\breve{u}(y) = 0. \tag{34}$$

Making change of variable $z = 2\hat{k}^{1/2}y$ and letting $f(z) = \breve{u}(y(z))$ so that (34) becomes $f_{zz} + z^2 f/4 = 0$. Two linearly independent solutions of this equation are given by (see Appendix A.2) $f_e = \Gamma(3/4)\hat{J}_{-1/4}\left(z^2/4\right)$ and $f_o = \Gamma(5/4)z\hat{J}_{1/4}\left(z^2/4\right)$, where $\hat{J}_\mu$ is the analytical part of J_μ (see (65)), the Bessel function of first kind of order μ (not to be confused with the same symbol used for growth rate). Going back to the original variable y, the following solves (34)

$$u_e = \Gamma(3/4)\,\hat{J}_{-1/4}(\hat{k}y^2), \quad u_o = \Gamma(5/4)\,y\hat{J}_{1/4}(\hat{k}y^2). \tag{35}$$

In turn, $exp(-\hat{k}y^2)u_e$ and $exp(-\hat{k}y^2)u_o$ solve $\mathcal{L}\tilde{u} = 0$. As a result, unique solution to (32) satisfying $\tilde{u}(\pm 1) = 0$ exists if and only if $J_{-1/4}(\hat{k}) \neq 0$ and $J_{1/4}(\hat{k}) \neq 0$, and given by

$$\left.\begin{aligned} \tilde{u} = e^{-\hat{k}y^2}u_e(y)\left(u_p(y)/u_e(y) - u_p(1)/u_e(1)\right), \\ u_p = u_o\int_0^y \psi u_e e^{\hat{k}s^2}ds - u_e\int_0^y \psi u_o e^{\hat{k}s^2}ds. \end{aligned}\right\} \tag{36}$$

Substitute (31) into the right hand side of $(25)_5$, $\hat{\tau}^{xy}$ can be solved with integration

$$\left.\begin{aligned} R^r_\eta \hat{\tau}^{xy} = (-|k|\hat{p}^+)e^{-|k|x}\tilde{\tau}^{xy}, \\ \tilde{\tau}^{xy} = (\tilde{u}_y + \psi_y\tilde{u})/\psi, \end{aligned}\right\} \tag{37}$$

where $\tilde{u}$ as in (36). Similarly, we obtain from $(25)_7$

$$\left.\begin{aligned} R^r_\eta De\hat{\tau}^{xx} = 2\hat{p}^+e^{-|k|x}\tilde{\tau}^{xx}, \\ \tilde{\tau}^{xx} = \left(\tilde{\tau}^{xy} + \hat{u}_y + 2\psi_y\hat{u}\right)\psi_y/\psi. \end{aligned}\right\} \tag{38}$$

The relation $R^r_\eta De\hat{\tau}^{xx}_x = -2\hat{p}^+|k|exp(-|k|x)\left(1 - \tilde{\tau}^{xy}_y\right)$ can also be obtained by substituting (27), $(26)_2$ and (37) into $(25)_3$. By (38), it must be $\tilde{\tau}^{xx} = 1 - \tilde{\tau}^{xy}_y$. As a result, the gap averaged of $R^r_\eta De\hat{\tau}^{xx}$ is given by (notice $\tilde{\tau}^{xy}$ is an odd function in y) $R^r_\eta De\langle\hat{\tau}^{xx}\rangle = 2\hat{p}^+(1 - \tilde{\tau}^{xy}(1))$ $exp(-|k|x)$, or equivalently by (37) together with $\tilde{u}(1) = 0$

$$R^r_\eta De\langle\hat{\tau}^{xx}\rangle = 2\hat{p}^+\left(1 - \tilde{u}_y(1)/\psi(1)\right)e^{-|k|x}. \tag{39}$$

6. Dispersion relation

Inserting $(19)_1$, (21), (27), (39), (31) into $(19)_3$ gives

$$R_\eta^r\mu\left(2\tilde{u}_y(1)/\psi(1)-1-\hat{p}^-/\hat{p}^+\right) = \left(|k|^3Ca^{-1}-3\langle U\rangle(R_\eta^r-R_\eta^l)|k|\right)\langle\tilde{u}\rangle. \tag{40}$$

Inserting (31), (22) into $(19)_2$ gives $\hat{p}^-/\hat{p}^+ = 3R_\eta^l\langle\tilde{u}\rangle/R_\eta^r$ so that (40) becomes

$$R_\eta^r\mu\left(2\tilde{u}_y(1)/\psi(1)-1\right)-3R_\eta^l\mu\langle\tilde{u}\rangle = \left(|k|^3Ca^{-1}-3\langle U\rangle(R_\eta^r-R_\eta^l)|k|\right)\langle\tilde{u}\rangle. \tag{41}$$

Recall $\tilde{u}$ given by (36) is linear in ψ, which is linear in μ by $(33)_2$, thus we may write

$$\tilde{u} = \mu De\, u_1(y;\hat{k}) + u_2(y;\hat{k}), \tag{42}$$

where u_1 and u_2 take on the form of (36) with ψ replaced with 1 and $1-\hat{k}/3+\hat{k}y^2$ respectively. Eliminating k in favor of $\hat{k}$ using $(30)_2$ from the right hand side of (41) and inserting (42), then multiplying by De gives

$$R_\eta^r\hat{\mu}\left(2\frac{\hat{\mu}u_{1,y}(1;\hat{k})+u_{2,y}(1;\hat{k})}{\hat{\mu}+M}-1\right)\cdots - 3R_\eta^l\hat{\mu}\left(\hat{\mu}\langle u_1\rangle+\langle u_2\rangle\right) = s\left(\hat{\mu}\langle u_1\rangle+\langle u_2\rangle\right), \tag{43}$$

where

$$\left.\begin{aligned}\hat{\mu}=\mu De,\quad s=\beta\hat{k}^3-2[\![R_\eta]\!]\hat{k},\quad [\![R_\eta]\!]=R_\eta^r-R_\eta^l\\ \beta=Ca^{-1}De^{-2}(3\langle U\rangle/2)^{-3},\quad M=1+2\hat{k}/3.\end{aligned}\right\} \tag{44}$$

After some algebra, (43) can be put in the following form

$$\left.\begin{aligned}\mathcal{F}(\hat{\mu},\hat{k},\beta,[\![R_\eta]\!])=0,\\ \mathcal{F}=f_3\hat{\mu}^3+f_2\hat{\mu}^2+f_1\hat{\mu}+f_0,\end{aligned}\right\} \tag{45}$$

where (R_η^l and R_η^r are eliminated in favor of $[\![R_\eta]\!]$ using $(44)_3$ and (7), i.e. $R_\eta^l+R_\eta^r=1$)

$$\left.\begin{aligned}f_3=3(1-[\![R_\eta]\!])/2,\\ f_2=s-z+f_3(M+x+z/3),\\ f_1=s(M+x)-yz+f_3(xM+yz/3),\\ f_0=sxM,\\ x=\langle u_2\rangle/\langle u_1\rangle,\\ y=(2u_{2,y}(1)-M)/(2u_{1,y}(1)-1),\\ z=(2u_{1,y}(1)-1)/\langle u_1\rangle.\end{aligned}\right\} \tag{46}$$

Notice the symbols x, y, z are reused and not to be confused with spatial variables. Since the coefficients $f_j=f_j(\hat{k},\beta,[\![R_\eta]\!])$ are known functions, all information about the roots of $\mathcal{F}$ are essentially known.

In analyzing the dispersion relation, three types of singular behavior are encountered and discussed in detail in Section 6.1. In Section 6.2, we show the recovery of the classical ST result [1] in the limit $De\to 0$. In Section 6.3, the dispersion relation is analyzed in detail for the case of air displacing an UCM fluid by taking the viscosity contrast $[\![R_\eta]\!]\to 1$ in (45). In Section 6.4, the more general case of a Newtonian fluid displacing an UCM fluid is considered, i.e. $[\![R_\eta]\!]\in(-1,1)$.

6.1. Three types of singular behaviors

6.1.1. Type I: Blow-up in the amplitude of velocity perturbation

Denote by $\{\alpha_j\}_{j=1}$ the set of positive zeros of $J_{-1/4}$ listed in increasing order, similarly denote by $\{\beta_j\}_{j=1}$ for $J_{1/4}$. It is shown in Appendix A.1 that both $\{\alpha_j\}_{j=1}$ and $\{\beta_j\}_{j=1}$ are infinite and interlaced in the following way $\alpha_1<\beta_1<\alpha_2<\beta_2\cdots$. When $\hat{k}=\beta_j$, the solution to the boundary value problem (32) is not unique, however this does not affect the dispersion relation because the non-unique part is odd and the interface condition only depends on the average of the solution. When $\hat{k}=\alpha_j$, the solution $\tilde{u}$ becomes unbounded. Expressing the right hand side of $(30)_2$ in dimensional form (superscript $*$) gives $\hat{k}=3|k^*|\lambda\langle U^*\rangle/2$, thus $\tilde{u}$ is singular when $1/|k^*|=3\lambda\langle U^*\rangle/(2\alpha_j)$. Since $\alpha_1\approx 2$, all such singular waves have wavelength less than 3/4 of the distance traveled by the fluid bulk within one fluid relaxation time. On the other hand, most of such singular waves, if not all, can be neglected because of a more fundamental limitation of the theory. In particular, the separation of lengths scales $L\gg b$ does not apply in the immediate vicinity of the interface where a fully three dimensional flow is expected. The theory becomes unreliable when the wavelength is comparable or smaller than the thickness of this region which is expected to be $\mathcal{O}(b)$ [5]. As a result, we restrict to $1/|k^*|\gg b$ for further development, which is equivalent to requiring $\hat{k}\ll 3\lambda\langle U^*\rangle/(2b)$. In a typical Hele-Shaw experiment, $b\sim\mathcal{O}(10^{-4}m)$, $\lambda\sim\mathcal{O}(10^{-1}s)$, and $\langle U^*\rangle$ is at most a few cm/s, rendering $3\lambda\langle U^*\rangle/(2b)\sim\mathcal{O}(10)$. Since $(\alpha_1,\alpha_2,\alpha_3)\approx(2,5,8)$, we focus on the following interval for the remainder of the paper.

$$\hat{k}\in(0,\alpha_1). \tag{47}$$

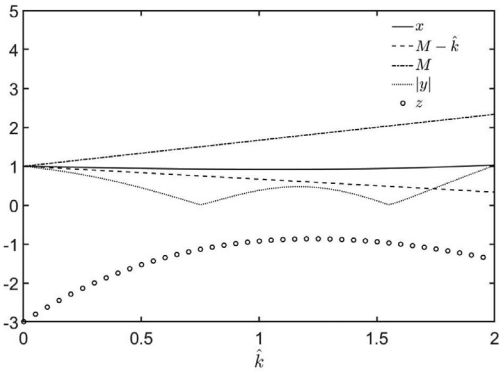

Fig. 2. Plots of the functions appearing in (48) v.s. $\hat{k}$, from which the inequalities clearly hold as well as the limiting values given by (49).

Remark 1. In Fig. 2, the function $M(\hat{k})$ given in (44), and $x(\hat{k})$, $y(\hat{k})$ and $z(\hat{k})$ given in (46) are plotted for $\hat{k}\in(0,\alpha_1)$, where the following clearly hold (they are important for later analysis and can be shown directly using analytical techniques but the proofs are lengthy thus omitted).

$$z<0<x,\quad M-\hat{k}<x<M,\quad |y|<x. \tag{48}$$

It is not difficult to show that in the limit $\hat{k}\to 0$ (this is also evident from Fig. 2)

$$x,y\to 1,\quad z\to -3. \tag{49}$$

6.1.2. Type II: Blow-up in the amplitude of stress perturbation

In obtaining (39) and subsequently (45), it is assumed that $\tilde{\tau}^{xy}$ is integrable over $y\in[-1,1]$ (here, y is the spatial variable and not to be confused with the y defined in (46)). However, this may not be true if ψ has a zero in $y\in[-1,1]$. By definition, $\psi\neq 0$ for all $y\in[-1,1]$ iff $\hat{\mu}\notin[-M,-M+\hat{k}]$. At this point, $\hat{\mu}$ is still unknown and hence this condition needs to be taken as a posterior restriction on the $\hat{\mu}$, once found. In other words, if a solution branch $\hat{\mu}=\hat{\mu}_j$ of (45) belongs to $[-M,-M+\hat{k}]$ for some combinations of $\hat{k}$, β and $[\![R_\eta]\!]$, then the stress associated with $\hat{\mu}_j$ can be unbounded at some points within $[-1,1]$ (at the zeros of ψ to be more precise). It is possible for the singularity to be removable if the zeros of the numerator of $\tilde{\tau}^{xy}$ coincide with that of ψ. It turns out that this is only the case when $\hat{\mu}=-M+\hat{k}$, not for other values of $\hat{\mu}$, i.e. $\tilde{\tau}^{xy}$ unbounded if $\hat{\mu}\in[-M,-M+\hat{k})$.

6.1.3. Type III: Blow-up in the growth rate $\hat{\mu}$

Since $\mathcal{F}$ given by (45) is a polynomial in $\hat{\mu}$, one of the roots must diverge if the leading coefficient f_3 vanishes. This can only happen when $[\![R_\eta]\!] = 1$, in which case $\mathcal{F}$ degenerates to a quadratic polynomial. For such limiting case, it turns out that if β is smaller than some critical value $\beta_* \approx 1.113$, the leading coefficient of the degenerated $\mathcal{F}$ can be zero at certain isolated wavenumbers where one of the roots becomes singular. This resembles a resonance phenomena and will be discussed in detail in Section 6.3.2.

6.2. Recovery of Saffman–Taylor result

The Newtonian limit is obtained by taking the limit $De \to 0$ so that $\hat{k} \to 0$ and $\psi \to 1$ by $(33)_2$. By definitions (35) and $(65)_2$, it is easy to see $u_e \to 1$ and $u_o \to y$ in this limit. As a result, (36) gives $\tilde{u} \to (y^2-1)/2$, thus $\tilde{u}_y(1) \to 1$ and $\langle \tilde{u} \rangle \to -1/3$. Substituting these limits into (41) and using $R_\eta^l + R_\eta^r := 1$ gives the classical ST [1] result in the following non-dimensional form (in Appendix A.6, the equivalent dimensional form is given)

$$\mu^{st} = -Ca^{-1}|k|^3/3 + \langle U \rangle [\![R_\eta]\!]|k|, \tag{50}$$

Provided $[\![R_\eta]\!] > 0$, the maximum growth rate $\mu_\dagger^{st}$ and the most unstable wavenumber $k_\dagger^{st}$ are given by

$$\mu_\dagger^{st} = \frac{2}{3}\sqrt{Ca\langle U \rangle^3 [\![R_\eta]\!]^3}, \quad k_\dagger^{st} = \sqrt{Ca\langle U \rangle [\![R_\eta]\!]}. \tag{51}$$

6.3. Air displacing an UCM fluid

In this section, we consider the special case where the displacing fluid is air instead of viscous Newtonian. It is customary to neglect all the associated dynamics on the air side. This is equivalent to taking $[\![R_\eta]\!] = 1$ in (45) and (46) resulting in

$$\mathcal{F}(\hat{\mu}, \hat{k}, \beta) = 0, \quad \text{where} \quad \mathcal{F} = f_2\hat{\mu}^2 + f_1\hat{\mu} + f_0, \tag{52}$$

and

$$\left.\begin{aligned} f_2 = s - z, \qquad f_1 = s(x+M) - yz, \\ f_0 = sMx, \qquad x = \langle u_2 \rangle / \langle u_1 \rangle, \\ y = (2u_{2,y}(1) - M)/(2u_{1,y}(1) - 1), \\ z = (2u_{1,y}(1) - 1)/\langle u_1 \rangle, \\ M = 1 + 2\hat{k}/3, \qquad s = \beta\hat{k}^3 - 2\hat{k}, \\ \beta = Ca^{-1}De^{-2}(3\langle U \rangle/2)^{-3}. \end{aligned}\right\} \tag{53}$$

Solving (52) gives

$$\left.\begin{aligned} \hat{\mu}_1(\hat{k}, \beta) = (-f_1 - \sqrt{\Delta})/(2f_2), \\ \hat{\mu}_2(\hat{k}, \beta) = (-f_1 + \sqrt{\Delta})/(2f_2), \\ \Delta = f_1^2 - 4f_0f_2. \end{aligned}\right\} \tag{54}$$

Such special case has been investigated first by Wilson [20] and later expanded by Mora and Manna [32]. Since no exact expressions such as (54) are obtained in their works due to the numerical method used, some features of the dispersion relation are not discovered or inadequately addressed. This is discussed further in Section 6.3.5.

In the long wave limit $\hat{k} \to 0$, $f_1, f_2 \to 3$, $f_0 \to 0$ by (49), thus $\hat{\mu}_1 \to -1$ and $\hat{\mu}_2 \to 0$. By continuity $\hat{\mu}_1$ remains to be negative for small $\hat{k}$. On the other hand, it is easy to show by (49) and continuity that $f_0 < 0 < f_1, f_2$ for small $\hat{k}$, thus $\hat{\mu}_2 > 0$ for small $\hat{k}$. As a result, we conclude instability for long waves.

6.3.1. Marginal stability curve

By definition (53), the coefficients $f_j(\hat{k}, \beta)$ are linear in β, thus $f_j = 0$ is given by an equation of the form $\beta = \varsigma_j(\hat{k})$. Using (48), it can be shown

$$\left.\begin{aligned} \{f_j \geq 0\}_{j=0}^2 = \{\beta \geq \varsigma_j(\hat{k})\}_{j=0}^2, \\ \{\Delta \leq 0\} = \{\varsigma_3 \leq \beta \leq \varsigma_4\}, \end{aligned}\right\} \tag{55}$$

where

$$\left.\begin{aligned} \varsigma_0 = \frac{2}{\hat{k}^2}, \quad \varsigma_1 = \varsigma_0 + \frac{z}{\hat{k}^3}\frac{y}{x+M}, \quad \varsigma_2 = \varsigma_0 + \frac{z}{\hat{k}^3}, \\ \varsigma_3 = \varsigma_0 - \frac{z}{\hat{k}^3}\left(\frac{\sqrt{(M-y)x} - \sqrt{M(x-y)}}{x-M}\right)^2, \\ \varsigma_4 = \varsigma_0 - \frac{z}{\hat{k}^3}\left(\frac{\sqrt{(M-y)x} + \sqrt{M(x-y)}}{x-M}\right)^2. \end{aligned}\right\} \tag{56}$$

The graphs of $\varsigma_j(\hat{k})$ for $j = 0, 1, 2, 3, 4$ are shown in Fig. 3. It also follows from (48) that

$$\varsigma_4 > \varsigma_3 > \varsigma_0 > \varsigma_2, \qquad \varsigma_4 > \varsigma_1 > \varsigma_2. \tag{57}$$

Claims 1 and 2 below describe the regions in $(\hat{k}, \beta)$ plane over which $\Re\{\hat{\mu}_2\}$ or $\Re\{\hat{\mu}_1\}$ is negative, which are illustrated in Figs. 4(a) and 4(b) respectively.

Claim 1: $\{\Re\{\hat{\mu}_2\} < 0\} = \{\beta < \varsigma_2\} \cup \{\max\{\varsigma_0, \varsigma_1\} < \beta\}$.

Proof. By Routh–Hurwitz stability criterion, both $\Re\{\hat{\mu}_1\}$ and $\Re\{\hat{\mu}_2\}$ are negative if and only if f_2, f_1, and f_0 have same sign, which is equivalent to $\beta < \min\{\varsigma_0, \varsigma_1, \varsigma_2\}$ or $\beta > \max\{\varsigma_0, \varsigma_1, \varsigma_2\}$ by $(55)_1$. As a result, by (57)

$$\{\Re\{\hat{\mu}_1\}, \Re\{\hat{\mu}_2\} < 0\} = \{\beta < \varsigma_2\} \cup \{\max\{\varsigma_1, \varsigma_0\} < \beta\}.$$

Provided $\beta \neq \varsigma_2$, taking complement of above gives $\{\Re\{\hat{\mu}_1\} \geq 0\} \cup \{\Re\{\hat{\mu}_2\} \geq 0\} = \{\varsigma_2 < \beta \leq \max\{\varsigma_1, \varsigma_0\}\}$. Since $\Re\{\hat{\mu}_1\} \leq \Re\{\hat{\mu}_2\}$ if $f_2 > 0$, which is equivalent to $\varsigma_2 < \beta$, $\{\Re\{\hat{\mu}_1\} \geq 0\} \cup \{\Re\{\hat{\mu}_2\} \geq 0\} = \{\Re\{\hat{\mu}_2\} \geq 0\} = \{\varsigma_2 < \beta \leq \max\{\varsigma_1, \varsigma_0\}\}$. Taking complement of this yields the result. ■

Claim 2: $\{\Re\{\hat{\mu}_1\} < 0\} = \{\beta < \varsigma_0\} \cup \{\varsigma_1 < \beta\}$.

Proof. We will find the set $\{\Re\{\hat{\mu}_1\} \geq 0\}$ instead and then take the complement. Since $\{\Delta \leq 0\} \cap \{\Re\{\hat{\mu}_1\} \geq 0\} = \{\Delta \leq 0\} \cap \{f_1/f_2 \leq 0\}$, which by (55)–(57), is equivalent to

$$\{\varsigma_3 \leq \beta \leq \varsigma_1\}. \tag{58}$$

Similarly, it is not difficult to show $\hat{\mu}_1 < 0$ if $f_2 \leq 0$, thus it suffices to consider $f_2 > 0$ and $\Delta \geq 0$, in particular

$$\begin{aligned} &\{\Re\{\hat{\mu}_1\} \geq 0\} \cap \{f_2 > 0\} \cap \{\Delta \geq 0\} \\ =&\left\{\sqrt{\Delta} \leq -f_1\right\} \cap \{f_2 > 0\} \cap \{\Delta \geq 0\} \\ =&\left\{\sqrt{\Delta} \leq -f_1\right\} \cap \{f_2 > 0\} \cap \{f_1 \leq 0\} \cap \{\Delta \geq 0\} \\ =&\{f_0 \geq 0\} \cap \{f_2 > 0\} \cap \{f_1 \leq 0\} \cap \{\Delta \geq 0\} \\ =&\{\beta \geq \varsigma_0\} \cap \{\beta > \varsigma_2\} \cap \{\beta \leq \varsigma_1\} \cap \{\{\beta \leq \varsigma_3\} \cup \{\varsigma_4 \leq \beta\}\} \\ =&\{\varsigma_0 \leq \beta \leq \min\{\varsigma_1, \varsigma_3\}\}. \end{aligned} \tag{59}$$

As a result $\Re\{\hat{\mu}_1\} \geq 0$ is given by (58) ∪ (59), which can be further reduced down to $\{\varsigma_0 \leq \beta \leq \varsigma_1\}$, and taking the complement yields the result. ■

6.3.2. Resonance

In continuation of the discussion made in Section 6.1.3, at least one of $\hat{\mu}_1$ or $\hat{\mu}_2$ will diverge if the leading coefficient f_2 vanishes. By (55)–(57), it is not difficult to show that only $\hat{\mu}_2$ diverges when $f_2 = 0$ (given by the equation $\beta = \varsigma_2(\hat{k})$). In addition, if the curve $\beta = \varsigma_2(\hat{k})$ (see Fig. 3(a)) is approached from above, then $\hat{\mu}_2 \to +\infty$, or $\hat{\mu}_2 \to -\infty$ if

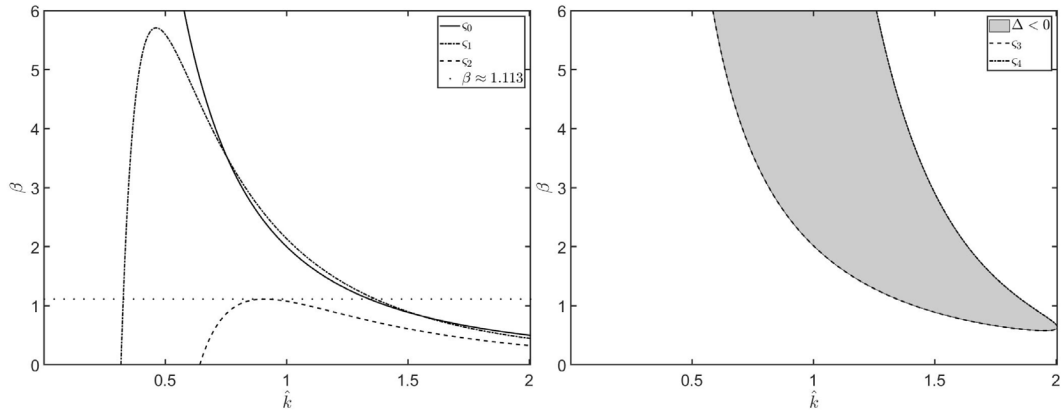

(a) (b)

Fig. 3. (a) For $j = 0, 1, 2$, $f_j > 0$ over the region above ς_j and $f_j < 0$ when below. The significance of dotted line $\beta = \beta_* \approx 1.113$ is discussed in Section 6.3.2. (b) $\hat{\mu}_1$ and $\hat{\mu}_2$ are complex conjugates inside the shaded region bounded by ς_3 and ς_4, and both real if outside.

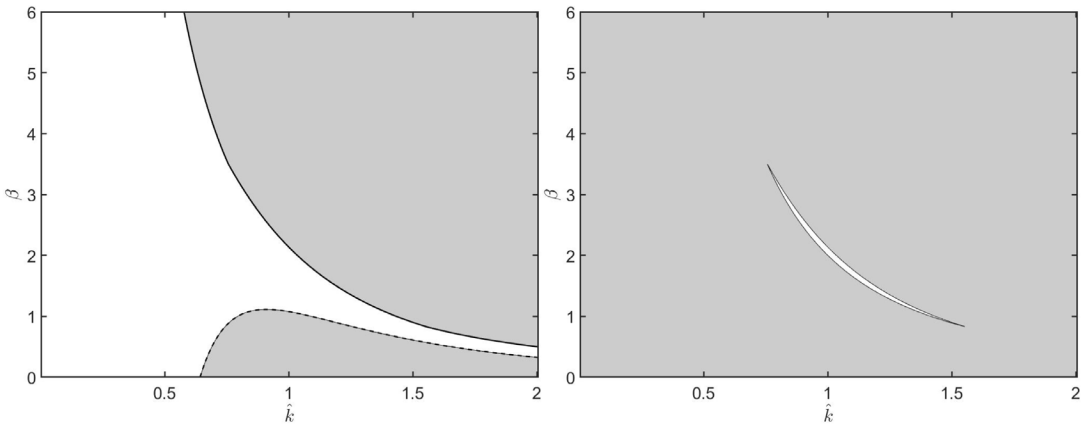

(a) $\Re\{\hat{\mu}_2\} < 0$ *over shaded region* (b) $\Re\{\hat{\mu}_1\} < 0$ *over shaded region*

Fig. 4. (a) $\hat{\mu}_2$ diverges over the dashed curve given by the equation $\beta = \varsigma_2$. The upper boundary is the marginal curve for $\hat{\mu}_2$ given by $\beta = \max\{\varsigma_0, \varsigma_1\}$. (b) The upper and lower boundary of the crescent region are the marginal curves for $\hat{\mu}_1$ given by $\beta = \varsigma_1$ and $\beta = \varsigma_0$ respectively.

Table 1
Resonating (modified) wavenumber for various β values.

β	1.113	1	0.8	0.5	0.4	0.3251	0.2	0.1	0
$\hat{k}_{\dagger,1}$	0.909	0.794	0.737	0.69	0.678	0.67	0.653	0.65	0.642
$\hat{k}_{\dagger,2}$	0.909	1.088	1.287	1.654	1.831	2	NA	NA	NA

approached from below. Solving $\beta = \varsigma_2(\hat{k})$ for $\hat{k}$ gives the associated singular (modified) wavenumber. It is clear from Fig. 3(a) that the solution is double-valued as ς_2 is not monotonic. Let $\hat{k}_{\dagger,1}$ and $\hat{k}_{\dagger,2}$ be the two solution branches, and wlog assume $\hat{k}_{\dagger,1} \le \hat{k}_{\dagger,2}$. The approximate values $\hat{k}_{\dagger,1}$ and $\hat{k}_{\dagger,2}$ for various values of β are given in (Table 1) ('NA' indicates the value is beyond region of interest, i.e. $\alpha_1 \approx 2.006$). The singular behavior only occurs when $\beta \le \beta_* = \max_{\hat{k}}\{\varsigma_2\} \approx 1.113$. To illustrate this, the plots of $\Re\{\hat{\mu}_2\}$ and $\Re\{\hat{\mu}_1\}$ v.s. $\hat{k}$ are given in Fig. 5 for various values of $\beta \le \beta_*$, where the singularities are clearly seen.

This singular behavior resembles a resonance phenomenon, where the temporal growth rate becomes unbounded when the wavenumber approaches certain value. Such resonance is also predicted in Mora and Manna [32], and a fracture-like pattern is observed in their experiment when β is smaller than β_*. However, the critical β value predicted by the authors is approximately 1.23 instead of $\beta_* \approx 1.113$ (after converting the analogous parameter from [32] to β used here). This discrepancy is most likely due to the power series method the authors used to solve the boundary value problem (see Section 5). On the other hand, the resonance can always be avoided by taking the flow speed sufficiently slow. To see this, we first express the right hand side of $(53)_9$ in dimensional terms (here, the superscript r is dropped on η^r)

$$\beta = \frac{8\gamma b^2}{27\eta\lambda^2\langle U^*\rangle^3} \quad \Rightarrow \quad \langle U^*\rangle = \frac{2}{3\beta^{1/3}}\left(\frac{\gamma}{\eta}\frac{b^2}{\lambda^2}\right)^{1/3}. \tag{60}$$

For a given experiment, the parameters b, η, λ and γ are fixed, thus taking $\beta = \beta_* \approx 1.113$ gives the critical velocity beyond which the resonance occurs. For example, using the parameters from [32] ($b = 2.5 \cdot 10^{-4}$ m, $\gamma = 3 \cdot 10^{-2}$ N/m, $\lambda \approx 1 \cdot 10^{-1}$ s, $\eta \approx 1 \cdot$ Ns/m^2) gives $\langle U^*\rangle \ge 3.682 \cdot 10^{-3}$ m/s.

6.3.3. Maximum growth rate and most unstable wave

When $\beta \le \beta_*$, the maximum growth rate is infinity as discussed in Section 6.3.2. For $\beta > \beta_*$ (implying $f_2 > 0$), we have $\Re\{\hat{\mu}_1\} \le \Re\{\hat{\mu}_2\}$. Let $\hat{k} = \hat{k}_\dagger(\beta)$ be modified wavenumber at which $\hat{\mu}_\dagger(\beta) = \max_{\hat{k}} \Re\{\hat{\mu}_2\}$ is attained. By definition $(44)_1$, $(30)_2$ and $(30)_3$, the maximum growth rate and the most unstable wavenumber are given by

$$\mu_\dagger = \hat{\mu}_\dagger(\beta)/De, \qquad k_\dagger = 2\hat{k}_\dagger(\beta)/(3De\langle U\rangle). \tag{61}$$

Let $\mu_\dagger^{st}$ and $k_\dagger^{st}$ be their Saffman-Taylor counterparts given by (51) (with $[\![R_\eta]\!] = 1$). Using definition of β given by $(53)_9$, we can write

$$\mu_\dagger/\mu_\dagger^{st} = (3/2)^{5/2}\sqrt{\beta}\,\hat{\mu}_\dagger(\beta), \quad k_\dagger/k_\dagger^{st} = \sqrt{3\beta/2}\,\hat{k}_\dagger(\beta).$$

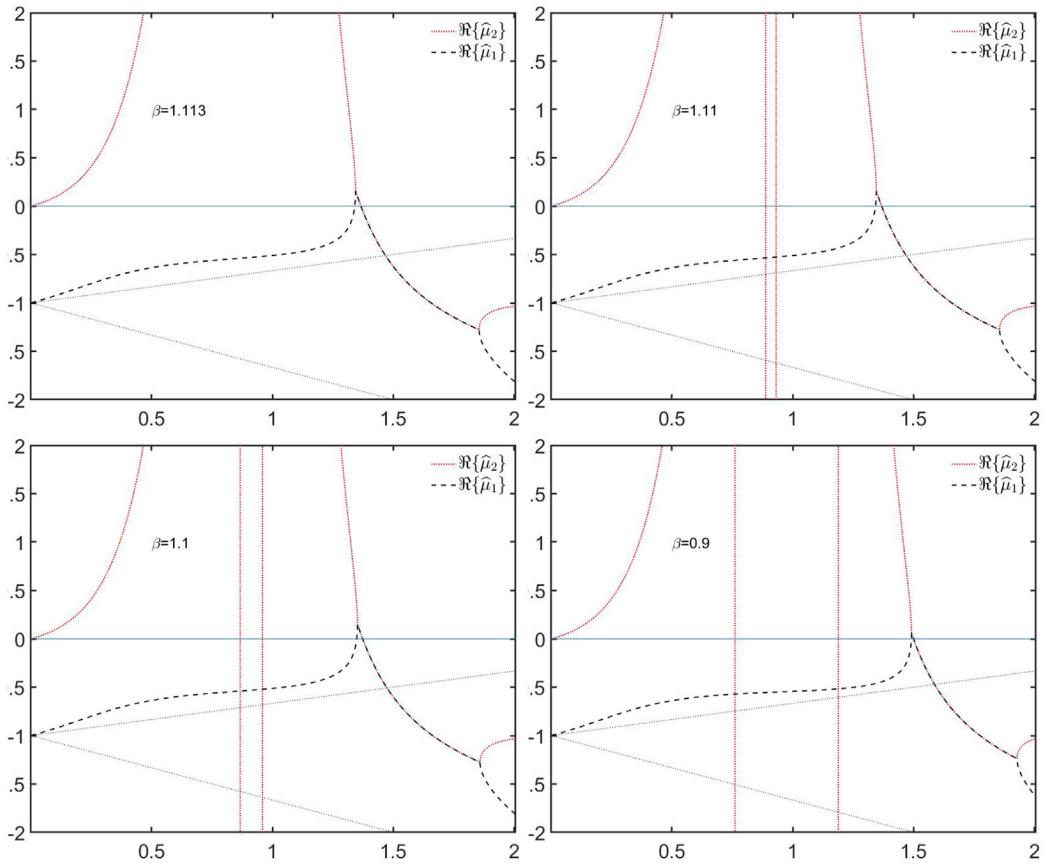

Fig. 5. Plots of $\Re\{\hat{\mu}_2\}$ and $\Re\{\hat{\mu}_1\}$ v.s. $\hat{k}$ for four values of $\beta \le \beta_* \approx 1.113$. The divergence occurs at $\hat{k} = \hat{k}_{\dagger,1}$ or $\hat{k} = \hat{k}_{\dagger,2}$ whose approximate values are given in Table 1. The two dotted lines are $-M$ and $-M + \hat{k}$ and their significance are explained later in Section 6.3.4.

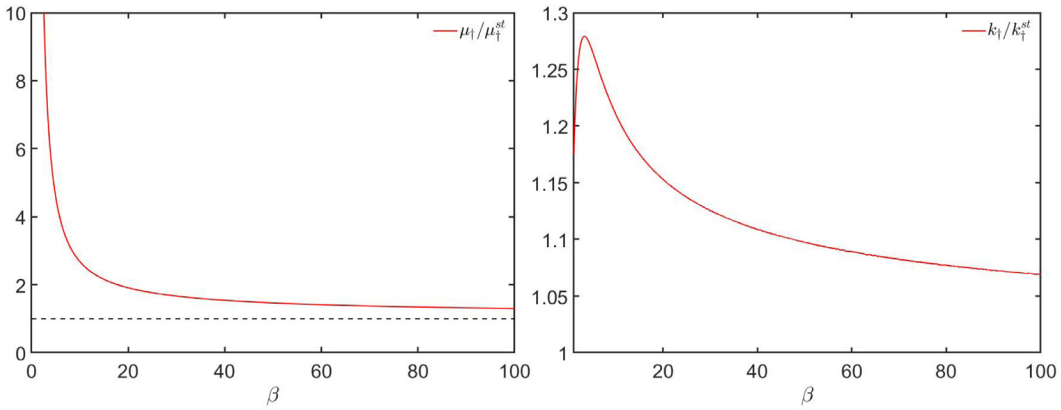

(a) $\mu_\dagger/\mu_\dagger^{st}$ *v.s.* β (b) $k_\dagger/k_\dagger^{st}$ *v.s.* β

Fig. 6. $\mu_\dagger$ and $k_\dagger$ are the maximum growth rate and the most unstable wavenumber. $\mu_\dagger^{st}$ and $k_\dagger^{st}$ are their Saffman–Taylor counterparts. Notice both ratios are larger than 1.

The plots of above two ratios are given in Fig. 6 which shows that both are bounded below by 1 for all β values. This implies (recall $(60)_1$) that for the same gap separation $2b$, interfacial tension γ, viscosity η and flow speed $\langle U^* \rangle$, the maximum growth rate is always larger than that of the ST case, and the most unstable wave has longer wavelength.

Now we consider the individual effect of Ca, De and $\langle U \rangle$ on $\mu_\dagger$. Notice $(\hat{k}_\dagger, \beta)$ must be contained in the unshaded region shown in Fig. 4(a), which in turn is contained in $\{\beta \le \varsigma_4\}$. It is shown in Claim 6 of Appendix A.4 that $\Re\{\hat{\mu}_2\}$ is strictly decreasing in β over $\{\beta \le \varsigma_4\}$, thus $\hat{\mu}_\dagger$ decreases as β increases. Since $\beta \propto Ca^{-1} De^{-2} \langle U \rangle^{-3}$, it follows that $\mu_\dagger$ decreases as Ca or $\langle U \rangle$ decreases. On the other hand, Fig. 6(a) shows $\mu_\dagger/\mu_\dagger^{st}$ decreases as β increases. Since $\mu_\dagger^{st}$ does not depend on De, it must be $\mu_\dagger$ decreases as De decreases.

The effects of decreasing any of Ca, De or $\langle U \rangle$ (with the other two being fixed) on $k_\dagger$ is similar to increasing β on $\hat{k}_\dagger$, $\beta^{1/2}\hat{k}_\dagger$ or $\beta^{1/3}\hat{k}_\dagger$ respectively. This is because by $(61)_2$

1. $k_\dagger \propto \hat{k}_\dagger(\beta)$ for fixed De and $\langle U \rangle$. Since $\beta \propto Ca^{-1}$, decreasing Ca is equivalent to increasing β.
2. For fixed Ca and $\langle U \rangle$, eliminating De from $(61)_2$ in favor of β gives $k_\dagger \propto \beta^{1/2}\hat{k}_\dagger(\beta)$. Since $\beta \propto De^{-2}$, decreasing De is equivalent to increasing β on $\beta^{1/2}\hat{k}_\dagger$.

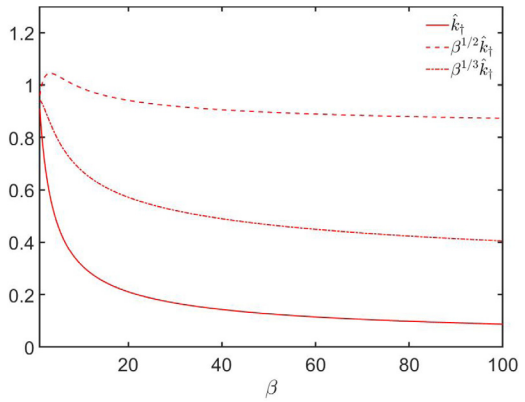

Fig. 7. Plots of $\hat{k}_\dagger$ (solid), $\beta^{1/2}\hat{k}_\dagger$ (dashed) and $\beta^{1/3}\hat{k}_\dagger$ (dash-dotted) v.s β.

3. For fixed Ca and De, eliminating $\langle U\rangle$ in favor of β gives $k_\dagger \propto \beta^{1/3}\hat{k}_\dagger(\beta)$. Since $\beta \propto \langle U\rangle^{-3}$, decreasing $\langle U\rangle$ is equivalent to increasing β on $\beta^{1/3}\hat{k}_\dagger$.

In Fig. 7, plots of $\hat{k}_\dagger$, $\beta^{1/2}\hat{k}_\dagger$ and $\beta^{1/3}\hat{k}_\dagger$ v.s. β are given. It then follows that $k_\dagger$ decreases as Ca or $\langle U\rangle$ decreases, and as De decreases, $k_\dagger$ increases first then decreases again.

6.3.4. Singularity in stress

In continuation of the discussion made in Section 6.1.2, the stress associated with $\hat{\mu}_j$ is singular when $\hat{\mu}_j \in [-M, -M+\hat{k})$. This will happen under conditions given in Claims 3 and 4 below (see Appendix A.4 for proofs). In Fig. 8, the regions where stress is singular are shown in $(\hat{k}, \beta)$ plane.

Claim 3: $\hat{\mu}_2 \in [-M, -M+\hat{k})$ if and only if $\{\beta \geq \varsigma_4\} \cup \{\max\{\varsigma_5, \varsigma_7\} < \beta \leq \varsigma_3\}$, where

$$\varsigma_5 = \varsigma_0 + \frac{\hat{k}-M}{\hat{k}}\frac{z}{\hat{k}^3}\frac{y+\hat{k}-M}{x+\hat{k}-M}, \quad \varsigma_7 = \varsigma_0 + \frac{z}{\hat{k}^3}\frac{y+2(\hat{k}-M)}{x+(2\hat{k}-M)}.$$

Claim 4: $\hat{\mu}_1 \in [-M, -M+\hat{k})$ if and only if

$$\{\varsigma_4 \leq \beta\} \cup \{\varsigma_7 \leq \beta \leq \varsigma_3\} \cdots \\ \cup \{\varsigma_2 < \beta < \min\{\varsigma_7, \varsigma_5, \varsigma_3\}\} \cup \{\beta < \min\{\varsigma_5, \varsigma_2\}\}.$$

Recall that the resonance phenomena discussed before can only happen at up to two isolated wavenumbers. However, the stress singularities can happen over a continuum of wavenumbers even when the velocities are well behaved. This counter-intuitive situation perhaps is a flaw of the UCM model. In its equivalent microscopic description, the model considers the fluid a dilute polymer solution with Newtonian solvent and the polymer particles are treated as Hookean dumbbells. The bulk velocity of the solution is the same as that of the solvent due to diluteness but the non-Newtonian part of the stress is computed from the statistical ensemble of the dumbbells which can be infinitely stretched [37–39] producing singular stress. Although UCM model does not take into account the Newtonian part of the stress contributed by the solvent which is expected to have certain regularizing effect, our preliminary findings show the singularity remains even when the Oldroyd-B model is used instead. This will be addressed in a future publication.

6.3.5. Comparison to previous works

In Wilson [20], a boundary value problem (BVP) analogous to (32) is solved numerically where the solution becomes unbounded when a parameter (analogous to $\hat{k}$) approaches to 16.05. After converting this value to ours, this is very close to $\alpha_1 \approx 2.006$ (first zero of $J_{-1/4}$). Although no further values of α_j are given, this omission is not severe because it is overshadowed by the limitation described in Section 6.1.1. Due to the numerical nature of the solution, no exact expression is available in [20] such as (36) which is then used in the interface condition to obtain the dispersion relation (52). It is unclear the author's numerical approach also yielded the double valued growth rate as only one branch is shown, and what happens after $\hat{k} >\approx 1$ is also not discussed. The maximum growth rate predicted in [20] increases sharply but remains finite as a parameter named W_1 increases. This parameter turns out to be equivalent to our β through $W_1 = \sqrt{288/(27\beta)}$. In Section 6.3.2, we see the growth rate becomes unbounded at certain wavenumber(s) when $\beta \leq \beta_* \approx 1.113$ or equivalently $W_1 \geq\approx 3.1$. Since Wilson only considered up to $W_1 = 2.5$, it is unclear the author knew the growth rate will eventually become singular (at two wavenumbers) for $W_1 \geq\approx 3.1$. Regardless, he referred this sharp increase a resonance phenomenon which we have followed suit. However, it appears Wilson had mistaken the resonance with the singular behavior associated with α_1 (notice occurrence of the resonance depends on β only whereas this singular behavior associated with α_1 depends on $\hat{k}$ only). In addition, no detailed analysis on the dependence of maximum growth rate and most unstable wavenumber on the involved parameters is given. The singularity in stress is briefly mentioned as a numerical finding but no detailed analysis is given.

Wilson's work was later expanded by Mora and Manna [32] who further complemented their theoretical results with experiments. Power series method is used in Mora and Manna [32] to solve the BVP analogous to (32). Although such method is analytic in nature, the associated recursive relation is not solved and a truncated series is used instead, upon which the non-slip condition is imposed. Since the well-posedness of the BVP is not addressed in [32], the truncated series may not converge, which it will not when $\hat{k} \in \{\alpha_j\}_{j=1}^{\infty}$, or needs fairly large number of terms to have reasonable convergence when $\hat{k}$ is near any of the α_js. Further, y appears in the solution through the combination $\hat{k}y^2$, thus convergence also becomes more difficult as $\hat{k}$ increases. The computed growth rate appears to be very different from ours when $\hat{k}$ becomes large, which may be due to the convergence issue explained above. The growth rate predicted is double valued in [32] but the part where they are complex conjugates is absent, and the issue of stress singularity is overlooked.

The predicted resonance in [32] occurs approximately when $\beta \approx 1.23$ or less rather than 1.113 (after converting the analogous parameter used by the authors formulation to ours). This discrepancy is most likely due to the power series method as well. In addition, it appears the authors may not have noticed that there are up to two resonating wavenumbers. The authors attributed the source of this resonance to the presence of normal stress τ^{xx}. This is not the case from our analysis, where the divergence is more of a coupled effect. The authors used Eq. (130) in [32] in an attempt to find the cause of the resonance, which is analogous to $(\hat{p} - De\langle\hat{\tau}^{xx}\rangle)\,\mu = (-Ca^{-1}k^2 + 3\langle U\rangle)\langle\hat{u}\rangle$ in our notations. However, the authors mistakenly dropped the $\langle\hat{u}\rangle$ term and argued that $\hat{p} - De\langle\hat{\tau}^{xx}\rangle$ will go to zero so that μ must diverge to balance the right hand side, being finite. But with the term $\langle\hat{u}\rangle$ coming into the equation, the argument fails because $\langle\hat{u}\rangle$ also depends on μ (linearly). Ultimately, the divergence is due to the fact that the leading quadratic coefficient f_2 can sometimes vanish. By back tracking the derivations, it can be seen the form of f_2 comes from the combined structure of the governing equations, not limited to one specific term.

6.3.6. Summary

Compared to the classical ST result, there are two modes of growth rather than one if the displaced Newtonian fluid is replaced by an UCM fluid. Similar to ST result, the flow is unstable to long waves. The marginal stability curve is also very close to that of ST. The maximum growth rate is always greater than that of ST and most unstable wave length is shorter. Further, there are up to two isolated wavenumbers at which the growth rate is unbounded for $\beta \leq\approx 1.113$. This strongly resembles a resonance phenomenon which is absent in ST. However this singular behavior can always be removed by taking the flow speed to be sufficiently slow. The stress is singular if the wavenumber is large.

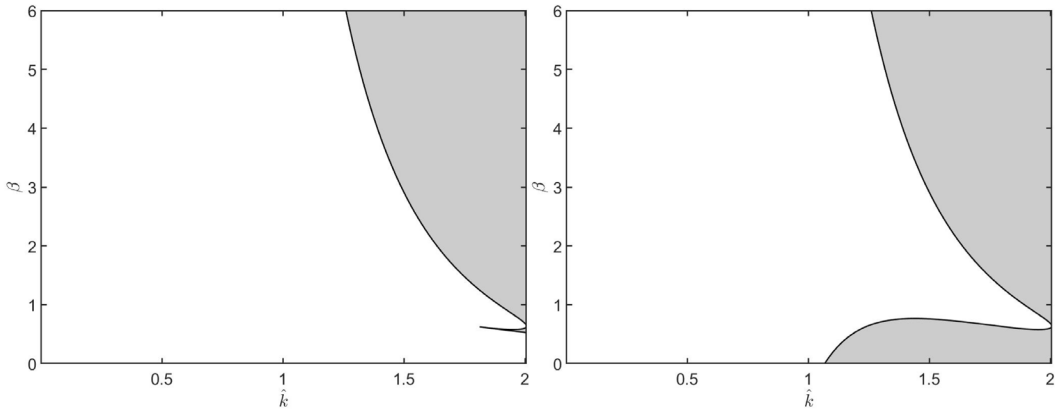

(a) $\hat{\mu}_2 \in [-M, -M+\hat{k})$ *in shaded region.* (b) $\hat{\mu}_1 \in [-M, -M+\hat{k})$ *in shaded region.*

Fig. 8. (a) Stress associated with $\hat{\mu}_2$ is singular over the shaded region with boundaries described in Claims 3. (b) Stress associated with $\hat{\mu}_1$ is singular over the shaded region with boundaries described in Claim 4.

6.4. A Newtonian fluid displacing an UCM fluid

At the beginning of Section 6, dispersion relation for this case is implicitly given by the cubic equation (45) in the modified growth rate $\hat{\mu}$ with coefficients $\{f_j\}_{j=0}^3$ given by (46), which depend on the modified wavenumber $\hat{k} > 0$ and $[\![R_\eta]\!] \in (-1, 1)$, $\beta > 0$ as parameters. The three roots $\{\hat{\mu}_j\}_{j=1}^3$ of $(45)_1$ can be found explicitly in terms of $\{f_j\}_{j=0}^3$ with cubic formula. It is proved in Appendix A.5 that for all $[\![R_\eta]\!] \in (-1, 1)$ and $\beta > 0$, one of the roots is always real and bounded above by $-M$, and the real parts of the other two are bounded below by $-M$. Without any loss of generality, we assume $\hat{\mu}_1 < -M < \Re\{\hat{\mu}_2\} \le \Re\{\hat{\mu}_3\}$. By (49) and definitions of f_js, it is straightforward to show $\{\hat{\mu}_j\}_{j=1}^3 \to \{-3/f_3, -1, 0\}$ in the limit $\hat{k} \to 0$. Since $f_3 > 0$ and by continuity, $\hat{\mu}_1$ and $\hat{\mu}_2$ are negative reals for small $\hat{k}$. This in turn implies, for small $\hat{k}$, $\hat{\mu}_3$ is also real and its sign is the same as that of $-f_0$ (because $f_3 > 0$). As a result, $\hat{\mu}_3 < 0$ for small $\hat{k}$ if and only if $[\![R_\eta]\!] \le 0$ (long wave instability if $[\![R_\eta]\!] > 0$) because $f_0 > 0$ for small $\hat{k}$ if and only if $[\![R_\eta]\!] \le 0$. In fact, it is shown in Section 6.4.1 that $[\![R_\eta]\!] \le 0$ is sufficient and necessary to have $\Re\{\hat{\mu}_j\} < 0$ for all $j = 1, 2, 3$ for all $\hat{k} > 0$ (up to $\alpha_1 \approx 2.006$). Notice $f_3 > 0$ for all $[\![R_\eta]\!] \in (-1, 1)$, thus the resonance described in Section 6.3.2 is removed. However, the singular behavior will be recovered in the limit $[\![R_\eta]\!] \to 1$ (provided $\beta \le \beta_* \approx 1.113$). See Fig. 9 for an illustration in support of this, where $\hat{\mu}_2^{au}$ in the figure refers to $\hat{\mu}_2$ defined in $(54)_2$ for the air displacing UCM case.

6.4.1. Marginal stability surface

Since $f_3 > 0$, Routh–Hurwitz criterion states $\Re\{\hat{\mu}_j\} < 0$ for $j = 1, 2, 3$ if and only if $f_0, f_2, f_2 f_1 - f_0 f_3 > 0$. By (48) and the definitions of f_js, this is equivalent to

$$s > 0, \qquad \mathcal{P}(s) > 0, \tag{62}$$

where

$$\left.\begin{aligned} \mathcal{P}(s) = s^2 + g_1 s + g_0, \quad r = \tfrac{1-[\![R_\eta]\!]}{1+[\![R_\eta]\!]} := \tfrac{\eta^l}{\eta^r}, \\ g_1 = \tfrac{3r(M+x)^2 - z(M+x+y)}{(1+r)(M+x)}, \quad g_0 = \tfrac{(3rxM - yz)(3r(M+x)-z)}{(1+r)^2(M+x)}. \end{aligned}\right\}$$

After some algebra, it can be shown that the discriminant of $\mathcal{P}$ is given by

$$\Delta_{\mathcal{P}} = \frac{9r^2(M-x)^2 - 6rz\left(\frac{M^2+x^2}{M+x} - y\right) + \left(z\frac{M+x-y}{M+x}\right)^2}{(1+r)^2}.$$

Since $g_1 > 0$ and $\Delta_{\mathcal{P}} > 0$ by (48), the two roots of $\mathcal{P}$ are real and one of them must be negative. As a result, (62) becomes $\max\{0, s_2\} < s$, where $s_2 = (-g_1 + \sqrt{\Delta_{\mathcal{P}}})/2$ is the larger root of $\mathcal{P}$, or equivalently (after inserting s given in $(44)_2$)

$$\left.\begin{aligned} \mathcal{M}(\hat{k}, [\![R_\eta]\!]) < \beta, \\ \mathcal{M} = 2[\![R_\eta]\!]/\hat{k}^2 + \max\{0, s_2(\hat{k}, [\![R_\eta]\!])\}/\hat{k}^3. \end{aligned}\right\} \tag{63}$$

The surface given by equation $\beta = \mathcal{M}(\hat{k}, [\![R_\eta]\!])$ is the marginal stability surface, above which (i.e. $\beta > \mathcal{M}$) the flow is stable and unstable if below ($\beta < \mathcal{M}$).

In Fig. 10, a few select curves over the marginal surface $\beta = \mathcal{M}(\hat{k}, [\![R_\eta]\!])$ are shown at fixed values of $[\![R_\eta]\!] > 0$. Evidently, increasing $[\![R_\eta]\!]$ or decreasing β will increase the unstable wave range. The limiting marginal curve as $[\![R_\eta]\!] \to 1$ is shown as the dashed curve, which is identical to the upper boundary of the shaded region in Fig. 4(a). To see this, it can be shown by (48) that $\mathcal{M} \to 2/\hat{k}^2 + \max\{0, yz/(M+x)\}/\hat{k}^3$ as $[\![R_\eta]\!] \to 1$, in turn $\beta = \mathcal{M}$ is simply the same as $\beta = \max\{\varsigma_0, \varsigma_1\}$, namely the second part of the union described in Claim 1 (the first part $\beta = \varsigma_2$ is missing due to the fact that this limit is degenerate in the sense $f_3 \to 0$).

Recall at the beginning of Section 6.4, it is shown that the condition $[\![R_\eta]\!] \le 0$ is necessary for $\Re\{\hat{\mu}_j\} < 0$ for $j = 1, 2, 3$ (for all $\hat{k}$). Now we show it is also a sufficient condition. Since $g_1 > 0$ by (48), $s_2 \le 0 \Leftrightarrow g_0 \ge 0 \Leftrightarrow yz/(3xM) \le r$. Numerical result shows the maximum of $yz/(3xM)$ is approximately 0.085. This implies if $[\![R_\eta]\!] \le 0$ (or equivalently $r \ge 1$) so that $s_2 < 0$, then $\mathcal{M}$ must be non-positive so that $(63)_1$ holds always. In other words, $[\![R_\eta]\!] \le 0$ implies $\Re\{\hat{\mu}_j\} < 0$ for $j = 1, 2, 3$.

By definition, $[\![R_\eta]\!] \le 0$ means the displacing fluid is more (or equally) viscous than the displaced fluid, therefore the viscosity contrast of the two fluid is still the decisive parameter in determining stability. This is similar to the ST case, where the growth rate is given by (50). The role of elasticity is the subject of the following subsections.

6.4.2. Maximum growth rate and most unstable wave

Let $\hat{k} = \hat{k}_\dagger^{nu}$ be the modified wavenumber at which $\hat{\mu}_\dagger^{nu} = \max_{\hat{k}} \Re\{\hat{\mu}_3\}$ is attained. We consider $[\![R_\eta]\!] > 0$ so that $\hat{\mu}_\dagger^{nu} > 0$. By definition, the maximum growth rate and the most unstable wavenumber are given by

$$\left.\begin{aligned} \mu_\dagger^{nu} = \hat{\mu}_\dagger^{nu}([\![R_\eta]\!], \beta)/De, \\ k_\dagger^{nu} = 2\hat{k}_\dagger^{nu}([\![R_\eta]\!], \beta)/(3De\langle U\rangle). \end{aligned}\right\} \tag{64}$$

The maximum growth rate $\mu_\dagger^{st}$ and the most unstable wavenumber $k_\dagger^{st}$ for the Saffman-Taylor case are given by (51), from which both Ca and $\langle U\rangle$ can be eliminated in favor of β defined by $(44)_4$. Consider the ratios

$$\left.\begin{aligned} \mu_\dagger^{nu}/\mu_\dagger^{st} = \sqrt{(3/2)^5\,\beta/[\![R_\eta]\!]^3}\,\hat{\mu}_\dagger([\![R_\eta]\!], \beta), \\ k_\dagger^{nu}/k_\dagger^{st} = \sqrt{(3/2)\,\beta/[\![R_\eta]\!]}\,\hat{k}_\dagger([\![R_\eta]\!], \beta). \end{aligned}\right\}$$

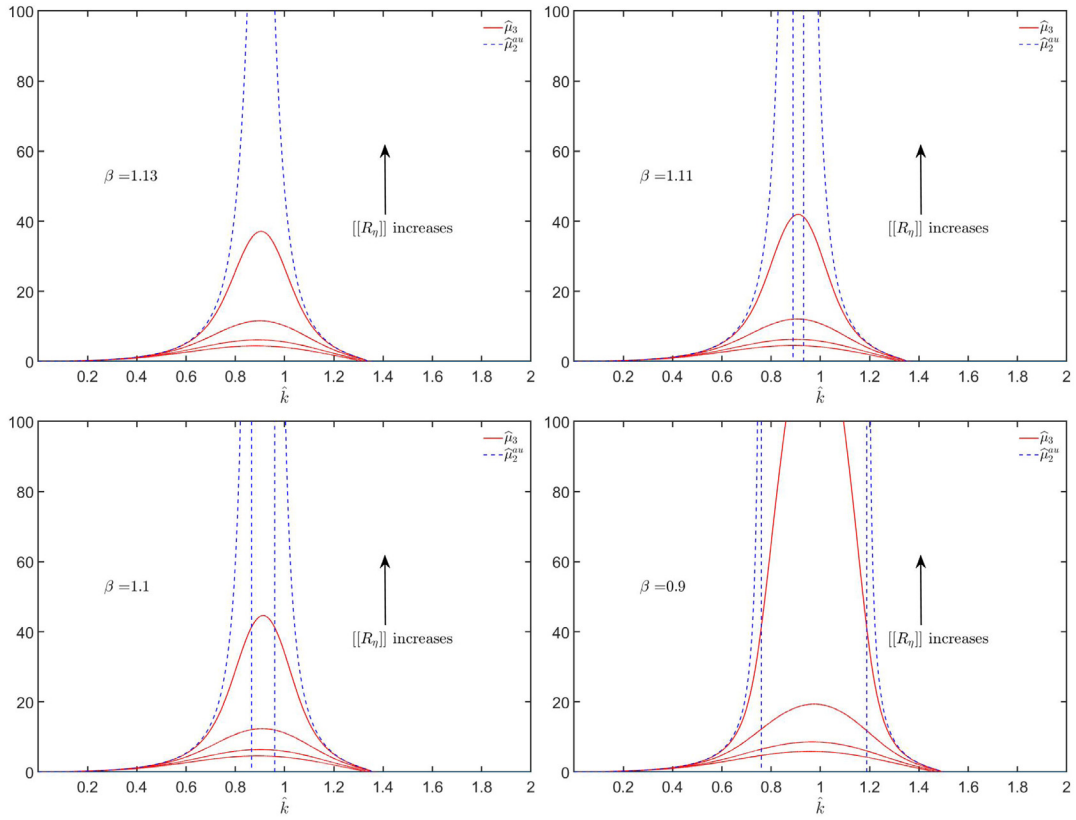

Fig. 9. In each sub-figure, $\hat{\mu}_3$ (solid) is plotted v.s. $\hat{k}$ at $[\![R_\eta]\!] = 0.95, 0.97, 0.99, 0.999$ (for the indicated β value). The dashed curve is the limit of $\hat{\mu}_3$ as $[\![R_\eta]\!] \to 1$, which is simply $\hat{\mu}_2^{nu}$.

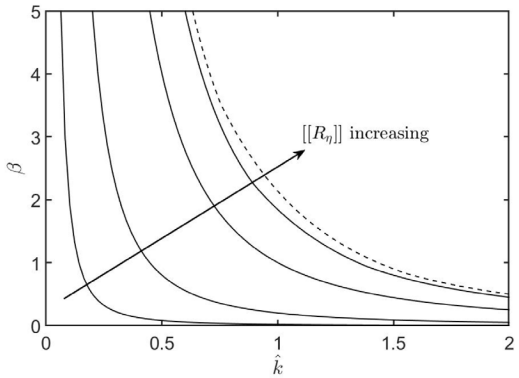

Fig. 10. Marginal stability curves (solid) at $[\![R_\eta]\!] = 0.01, 0.1, 0.5, 0.8$. The dashed curve is in the limit $[\![R_\eta]\!] \to 1$, which is identical to the upper boundary of the shaded region in Fig. 4(a). At each fixed $[\![R_\eta]\!]$ values, the flow is stable over the region above the associated marginal curves.

Above ratios are plotted in Fig. 11 as a function of β for various fixed $[\![R_\eta]\!]$ values. It is found $\mu_\dagger^{nu}/\mu_\dagger^{st} > 1$ for all $[\![R_\eta]\!] > 0$ and β. In other words, the displacement of an UCM fluid by a Newtonian fluid is always more unstable than the ST case (provided all parameters such as gap separation, surface tension, etc are same). Furthermore, as long as the parameter β is not too small $k_\dagger^{nu}/k_\dagger^{st}$ is also larger than 1, implying the most unstable wave has shorter wavelength than the ST case.

Now we turn to the individual effects of $[\![R_\eta]\!]$, Ca, De and $\langle U\rangle$ on $\mu_\dagger^{nu}$ and $k_\dagger^{nu}$ (recall $\beta \propto Ca^{-1}De^{-2}\langle U\rangle^{-3}$).

1. For fixed Ca, De and $\langle U\rangle$ (so that β is constant), it follows from $(64)_1$ that increasing $[\![R_\eta]\!]$ has the same effect on $\mu_\dagger^{nu}$ as it does on $\hat{\mu}_\dagger^{nu}$. From Fig. 12(a), we conclude that $\mu_\dagger^{nu}$ increases as $[\![R_\eta]\!]$ increases.
2. Similarly, for fixed De and $[\![R_\eta]\!]$, decreasing Ca or $\langle U\rangle$ will decrease $\mu_\dagger^{nu}$ because the effects are equivalent to increasing β on $\hat{\mu}_\dagger^{nu}$.
3. For fixed Ca, $\langle U\rangle$ and $[\![R_\eta]\!]$, we may eliminate the factor De^{-1} from $(64)_1$ in favor of β so that $\mu_\dagger^{nu} \propto \beta^{1/2}\hat{\mu}_\dagger^{nu}$. As a result, the effect of decreasing De on $\mu_\dagger^{nu}$ is equivalent to increasing β on $\beta^{1/2}\hat{\mu}_\dagger^{nu}$. From Fig. 13(a), we see as De decreases, $\mu_\dagger^{nu}$ increases first sharply then decreases.
4. From $(64)_2$, Fig. 12(b) and applying similar arguments as in #1 above, we conclude $k_\dagger^{nu}$ increases as $[\![R_\eta]\!]$ increases.
5. For fixed De, $\langle U\rangle$ and $[\![R_\eta]\!]$ so that $k_\dagger^{nu} \propto \hat{k}_\dagger^{nu}$ by $(64)_2$. Thus decreasing Ca for $k_\dagger^{nu}$ is equivalent to increasing β for $k_\dagger^{nu}$. From Fig. 12(b), we conclude decreasing Ca decreases $k_\dagger^{nu}$.
6. Fixing Ca, $\langle U\rangle$ and $[\![R_\eta]\!]$ and eliminate De^{-1} from $(64)_2$ in favor of β, then $k_\dagger^{nu} \propto \beta^{1/2}\hat{k}_\dagger^{nu}$. Thus decreasing De on $k_\dagger^{nu}$ is equivalent to increasing β on $\beta^{1/2}\hat{k}_\dagger^{nu}$. From Fig. 13(b), we see as De decreases, $k_\dagger^{nu}$ increases sharply first then decreases slowly.
7. Fixing Ca, De and $[\![R_\eta]\!]$ and eliminate $\langle U\rangle^{-1}$ from $(64)_2$ in favor of β, then $k_\dagger^{nu} \propto \beta^{1/3}\hat{k}_\dagger^{nu}$. Thus decreasing $\langle U\rangle$ on $k_\dagger^{nu}$ is equivalent to increasing β on $\beta^{1/3}\hat{k}_\dagger^{nu}$. From Fig. 13(b), we see as $\langle U\rangle$ decreases, $k_\dagger^{nu}$ increases sharply first then decreases slowly.

6.4.3. *Singularity in stress*

Recall from Section 6.1.2 that the stress associated with $\hat{\mu}_j$ is singular if $\hat{\mu}_j \in [-M, -M+\hat{k})$. It has been established in the beginning of Section 6.4 that $\hat{\mu}_1 < -M < \Re\{\hat{\mu}_2\} \le \Re\{\hat{\mu}_3\}$ for all $\beta > 0$ and $[\![R_\eta]\!] \in (-1, 1)$, thus it suffices to consider $\hat{\mu}_2$ only. In other words, we need to determine the condition for which $-M+\hat{k} \le \hat{\mu}_2$ (this implicitly requires

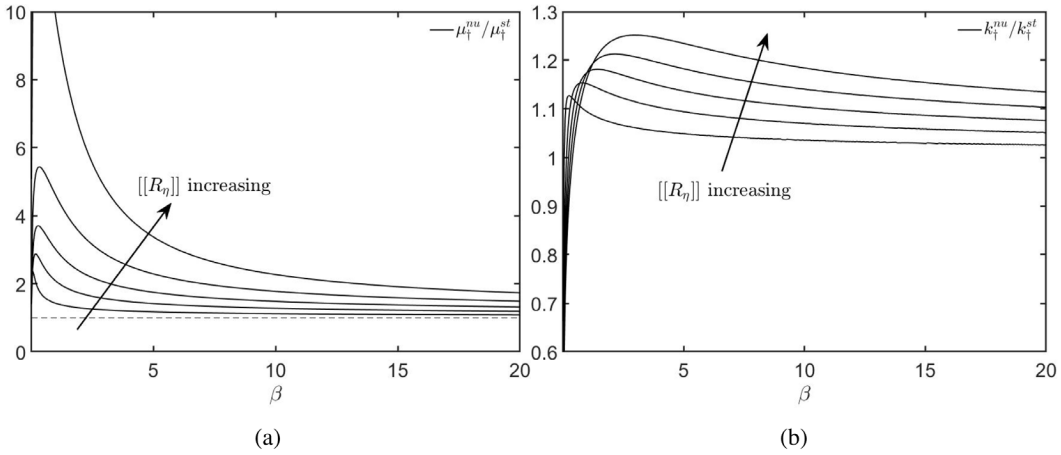

Fig. 11. Plots of $\mu_\dagger^{nu}/\mu_\dagger^{st}$ and $k_\dagger^{nu}/k_\dagger^{st}$ v.s. β for $[\![R_\eta]\!] = 0.1, 0.3, 0.5, 0.7, 0.9$.

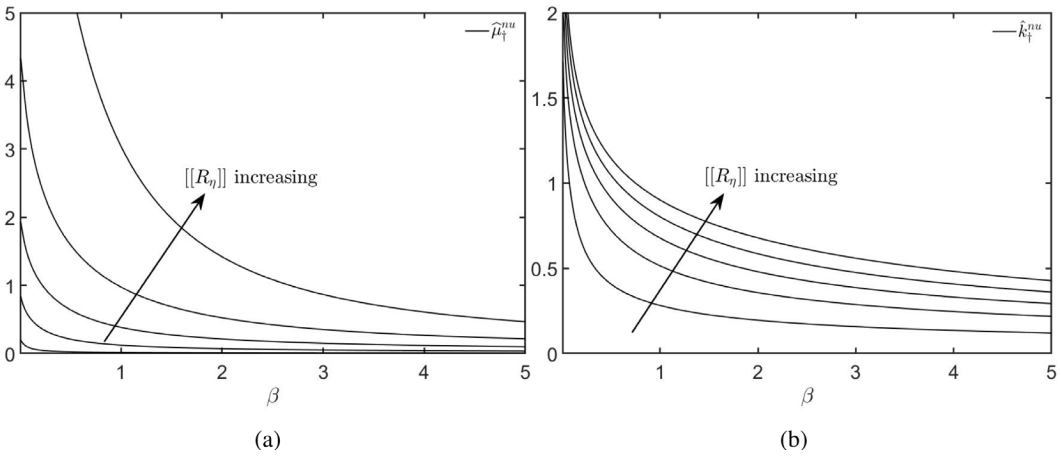

Fig. 12. Plots of $\hat{\mu}_\dagger$ and $\hat{k}_\dagger$ versus β for $[\![R_\eta]\!] = 0.1, 0.3, 0.5, 0.7, 0.9$.

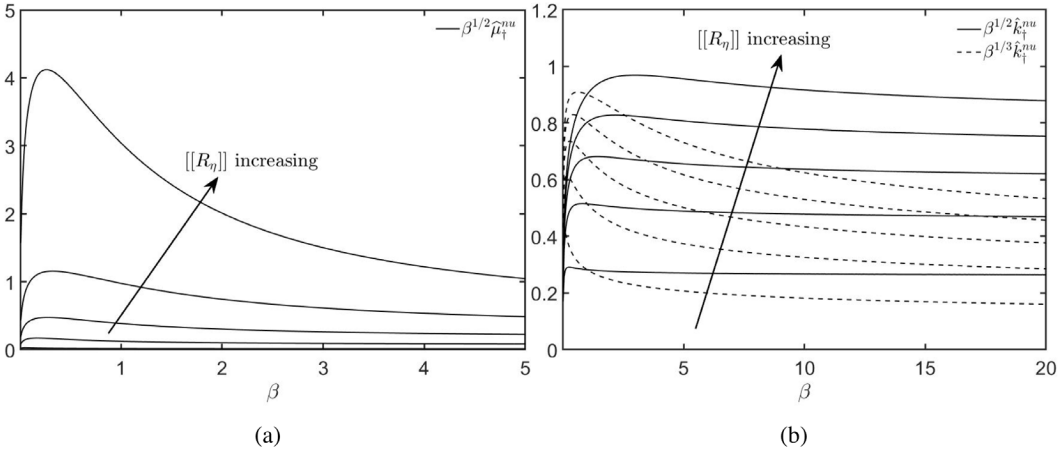

Fig. 13. Plots of $\beta^{1/2}\hat{\mu}_\dagger$, $\beta^{1/2}\hat{k}_\dagger$ and $\beta^{1/3}\hat{k}_\dagger$ versus β for $[\![R_\eta]\!] = 0.1, 0.3, 0.5, 0.7, 0.9$.

$\hat{\mu}_2$ to be real). Since $\hat{\mu}_2 = \hat{\mu}_2(\hat{k}, \beta, [\![R_\eta]\!])$, this inequality represents a region bounded by some surface in $(\hat{k}, \beta, [\![R_\eta]\!])$ space. In Fig. 14 and Fig. 15, a few select curves on this surface are shown for several fixed values of $[\![R_\eta]\!]$. In the regions labeled 'NS', stress for both $\hat{\mu}_2$ and $\hat{\mu}_3$ are non-singular, whereas in 'S' regions at least one of them corresponds to singular stress. For each fixed $[\![R_\eta]\!]$ and β, the stress for either $\hat{\mu}_2$ or $\hat{\mu}_3$ is never singular for small $\hat{k}$ but becomes singular when $\hat{k}$ is larger than some value of $\hat{k}_3$ which depends on $[\![R_\eta]\!]$ and β. If $[\![R_\eta]\!] <\approx -0.64$ and β is relatively small, there can be a second branch of singular wave band $(\hat{k}_1, \hat{k}_2)$. For example when $[\![R_\eta]\!] = -0.75$ and $\beta = 2$ (see the top left subfigure of Fig. 14), $\hat{k}_1 \approx 0.36$, $\hat{k}_2 \approx 0.55$ and $\hat{k}_3 \approx 1.12$. The interval $(\hat{k}_1, \hat{k}_2)$ shrinks as β increases and eventually disappears when $\beta >\approx 3.19$.

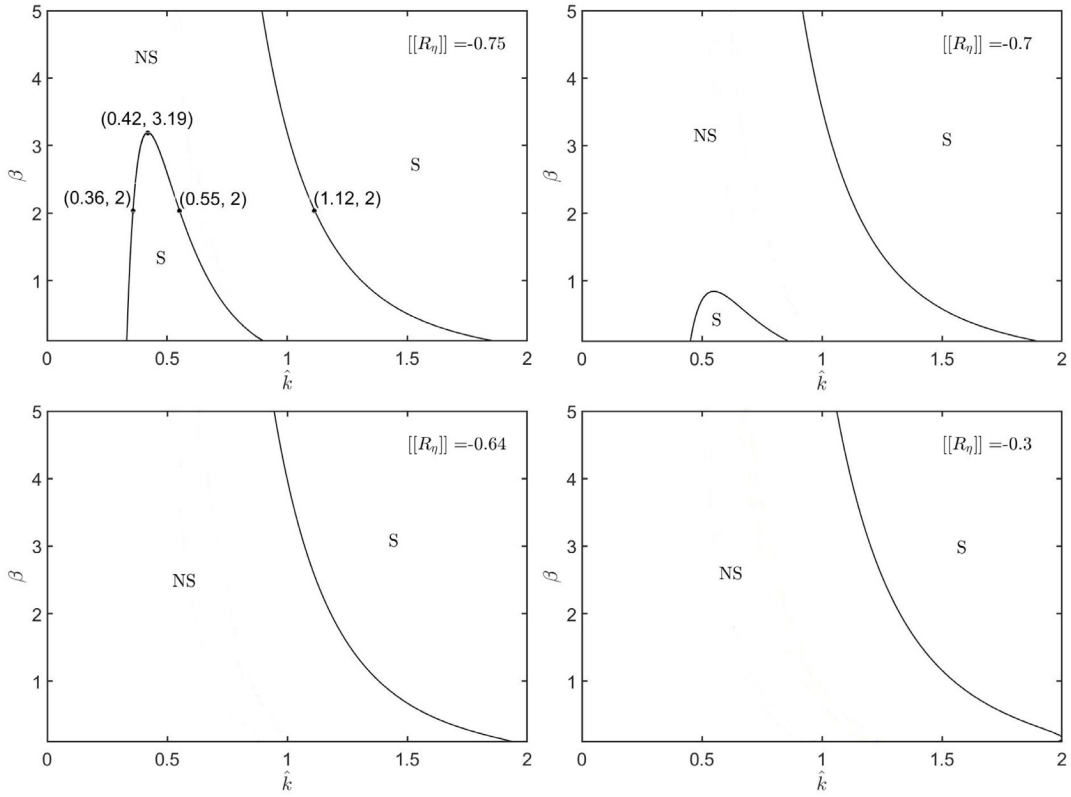

Fig. 14. In each of above subfigures, for the indicated $[\![R_\eta]\!]$ value, the region where the inequality $-M + \hat{k} \leq \hat{\mu}_2(\hat{k}, \beta, [\![R_\eta]\!])$ holds is labeled as 'NS', and 'S' otherwise. The 'NS' regions are where the stress associated with both $\hat{\mu}_2$ and $\hat{\mu}_3$ are non-singular, whereas the stress associated with at least one of them will be singular in the 'S' regions. In Fig. 15, 'NS' and 'S' regions are shown for additional $[\![R_\eta]\!]$ values.

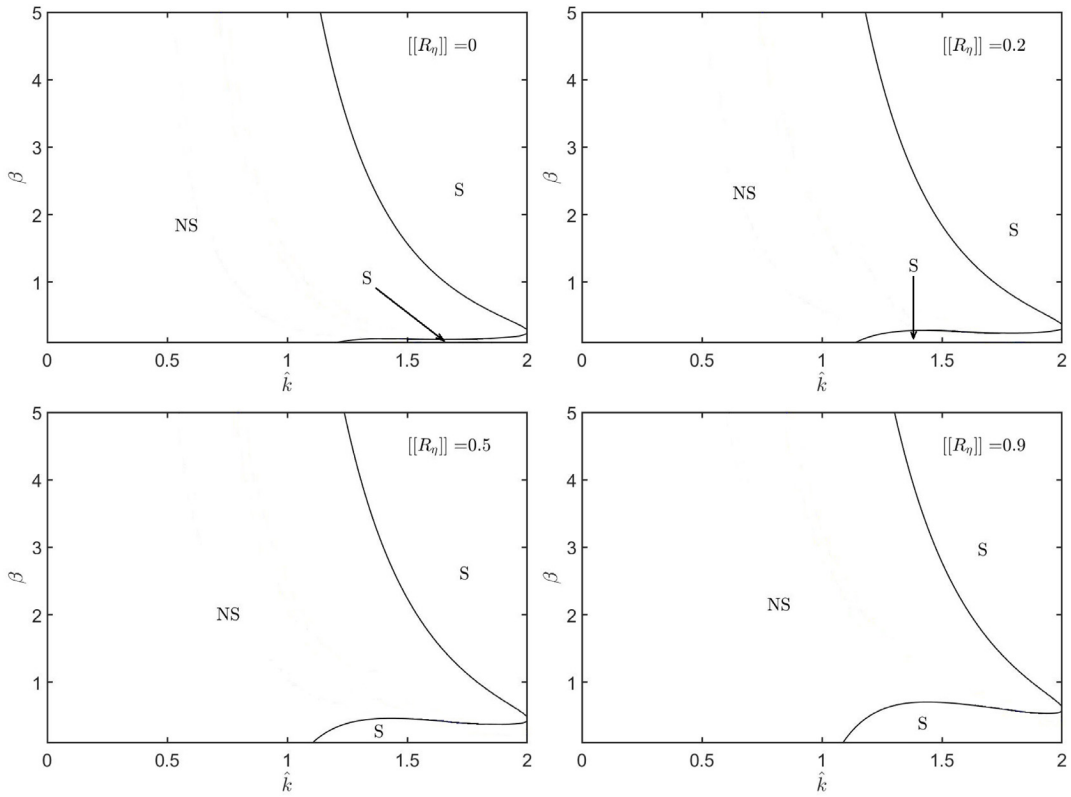

Fig. 15. In continuation of Fig. 14, 'NS' or 'S' regions are shown for additional $[\![R_\eta]\!]$ values.

6.4.4. Summary

Compared to the air displacing UCM case, there are three modes of growth rather than two and the resonance is removed. The mode ($\hat{\mu}_1$) is always stable for all parameter values, in particular the viscosity contrast, Capillary number, Deborah number and flow speed. In addition, the stress associated with this mode is never singular. The other two modes ($\hat{\mu}_2$ and $\hat{\mu}_3$) are both stable if and only if the viscosity of the Newtonian fluid (displacing) is higher or equal to that of the UCM fluid (displaced). Interestingly, viscosity is still the decisive factor in this regard just like the ST case. However, the stress associated with these two modes can become singular for large wavenumbers thus this stability criterion is only valid up to the wavenumber before they become singular. If the UCM fluid is more viscous, one of these two modes ($\hat{\mu}_3$) becomes unstable for long waves, and increasing the viscosity further makes such unstable long wave band wider. The maximum growth rate is always larger than that of the ST case, and (almost always) achieved at a shorter wavelength. Decreasing the viscosity of the UCM fluid, Capillary number, Deborah number, or flow speed decreases (almost always) the maximum growth rate (but remains positive) and makes the most unstable wave length longer.

7. Conclusions

In an attempt to find the role of elasticity on the formation of fingering instability, we considered the Saffman–Taylor (ST) problem in a rectilinear Hele-Shaw cell where an UCM fluid is displaced by a Newtonian fluid. A set of reduced equations is first derived in the thin gap limit through a proper scaling scheme while preserving the elastic feature of the UCM fluid. These equations are subsequently linearized about the steady state unidirectional flow and the method of normal mode is then employed. This leads to a classical two point boundary value problem (BVP) for the amplitude of the velocity disturbance which is then solved analytically. The solution is then inserted into the interface conditions from which we find that the dispersion relation is implicitly given by a cubic equation. The coefficients depend on the wavenumber k, viscosity ratio η^r/η^l, Deborah number De, Capillary number Ca and flow speed $\langle U\rangle$, and the temporal growth rate is given by the three roots $\{\mu_j\}_{j=1}^3$ of the cubic polynomial where the classical ST result is recovered in the small Deborah number limit $De \to 0$. Viscosity ratio is still the decisive factor in determining stability just like the ST case in the sense that the real parts of μ_js are all negative if and only if $\eta^r/\eta^l \le 1$. As η^r/η^l exceeds the threshold 1, long waves become unstable and increasing this ratio makes the unstable wave range wider. The maximum growth rate is always larger than that of the ST case and (almost always) achieved at a shorter wavelength. Decreasing η^r/η^l, Ca, De, or $\langle U\rangle$ (almost always) decreases the maximum growth rate and increases the wavelength of the most unstable wave. There is a sharp increase, but remains finite, of the maximum growth rate when η^r/η^l becomes very large. These behaviors persist up to the limit $\eta^l \to 0$, where it has the natural physical interpretation that the displacing fluid is replaced with air owing to the thin gap limit. The most striking difference found in this limiting case (v.s. $\eta^l > 0$) is that the maximum growth rate becomes singular at up to two finite wavenumbers when the parameter group $\beta = 1/(CaDe^2(3\langle U\rangle/2)^3)$ becomes less than approximately 1.113. This singular behavior strongly resembles a resonance phenomenon, however it can always be avoided by keeping the flow sufficiently slow.

Besides the resonance phenomenon just mentioned, there arises a second type of singular behavior. In particular, the solution of the BVP becomes unbounded at infinitely many isolated wavenumbers. To be more precise, the singularity occurs if the wavelength of the disturbance is proportional to the distance traveled by the fluid bulk per fluid relaxation time. The proportionality constant is given by $3/(2\alpha_j)$ where α_j is the jth positive zero of Bessel function of first kind of order $-1/4$. Given a typical set of experimental parameters used in Hele-Shaw experiments, the wavelengths of all such singular waves are on the order of a millimeter or less and hence this singular behavior affects only shortwaves. There is also a third type of singularity that results in unbounded stress at two layers within the cell gap, both of which are parallel to the cell plates and symmetrically located about the middle plane. This is perhaps the worst type because it can happen over a continuum of wavenumbers, wheres the previous two can only happen at isolated wavenumbers. The mathematical origin of this is similar in nature to the one found in Rayleigh's equation [40], which is associated with the continuous part of the spectrum. Considering the full initial value problem appears to be necessary to resolve such issues but our effort has not been successful so far. Another possible reason is that this is simply a flaw of the UCM model because this singular behavior can happen even when the velocity is well behaved. In its equivalent microscopic description, the model considers the fluid a dilute polymer solution with Newtonian solvent and the polymer particles are treated as Hookean dumbbells. The bulk velocity of the solution is the same as that of the solvent due to diluteness but the non-Newtonian part of the stress is computed from the statistical ensemble of the dumbbells which can be infinitely stretched [37–39] producing singular stress. Although UCM model does not take into account the Newtonian part of the stress contributed by the solvent which is expected to have certain regularizing effect, our preliminary findings show the singularity remains even when the Oldroyd-B model is used instead.

Declaration of competing interest

The authors declare that they have no known competing financial interests or personal relationships that could have appeared to influence the work reported in this paper.

Acknowledgments

We sincerely thank the two reviewers for their excellent comments which have helped us to improve this paper considerably. Financial support from departmental graduate office to the author ZH and from the U.S. National Science Foundation through grant DMS-1522782 to the author PD is gratefully acknowledged.

Appendix A

In Appendix A.1 and Appendix A.2, the symbol z, ξ and μ represent generic complex variables and $\nu = -1/4$. For Appendix A.4 and Appendix A.5, z represents the function (of $\hat{k}$) given in (46).

A.1. Bessel functions

Let J_μ be the Bessel function of first kind of order $\mu \in \mathbb{C}$ given by

$$J_\mu(z) = \left(\frac{z}{2}\right)^\mu \hat{J}_\mu(z), \quad \hat{J}_\mu(z) = \sum_{n=0} \frac{(-1)^n (z/2)^{2n}}{n!\Gamma(\mu+n+1)}. \tag{65}$$

The following identity is well known

$$J'_{-\mu}J_\mu - J_{-\mu}J'_\mu = -2\sin(\mu\pi)/(\pi z). \tag{66}$$

From [41] (pg.479–482), all zeros (infinitely many) of J_ν are positive reals (recall $\nu = -1/4$). Except for $z = 0$, same holds for $J_{-\nu}$. Let α_j be the jth positive zeros of J_ν arranged in ascending order and similarly define β_j for $J_{-\nu}$.

Claim: $0 < \alpha_1 < \beta_1 < \alpha_2 < \beta_2 \cdots$

Proof. We first show $\alpha_j \neq \beta_j$ for all j. Suppose otherwise, and let $\alpha_j = \beta_j$ for some j. It is well known that zeros of Bessel functions are always simple (regardless of the kind and order) except possibly at the origin. This implies $z = \alpha_j$ must be a removable singularity of $J_{-\nu}/J_\nu$. However $(J_{-\nu}/J_\nu)' = \sqrt{2}/(\pi z J_\nu^2)$ by (66), which diverges at $z = \alpha_j$, thus a contradiction. Since $(J_{-\nu}/J_\nu)' > 0$ over $z \in (0, \alpha_1)$, and $J_{-\nu}/J_\nu \to 0$ as

$z \to 0^+$ by the defining series, it must be $\alpha_1 < \beta_1$. Consider $z \in (\alpha_j, \alpha_{j+1})$ for some $j \geq 1$. Since $J_{-\nu}/J_\nu$ is strictly increasing over such interval and diverges at both end points, it must be $J_{-\nu}/J_\nu \to -\infty$ as $z \to \alpha_j^+$ and understanding $J_{-\nu}/J_\nu \to \infty$ as $z \to \alpha_{j+1}^-$. By intermediate value theorem and strict monotonicity, there exists an unique point in (α_j, α_{j+1}) at which $J_{-\nu}/J_\nu = 0$, which in turn must be a zero of $J_{-\nu}$. Since j is arbitrary, the claim follows. ■

A.2. Weber's equation

The Weber's equation [42] (pg. 686) is given by

$$f_{\xi\xi} - \xi^2 f/4 = 0. \tag{67}$$

Two independent solutions are (recall $\nu = -1/4$)

$$f_1(\xi) = e^{-\xi^2/4} M\left(\nu + 1/2, 2\nu + 1, \xi^2/2\right),$$
$$f_2(\xi) = \xi e^{-\xi^2/4} M\left(-\nu + 1/2, -2\nu + 1, \xi^2/2\right),$$

where $M(a, b, \xi)$ is the confluent hypergeometric function. Under change of variable $z = \xi/c$ for some constant c, Eq. (67) becomes $f_{zz} - c^4 z^2 f/4 = 0$. Choosing $c^2 = i$ or $c^2 = -i$ gives the equation

$$f_{zz} + z^2 f/4 = 0, \tag{68}$$

whose two linearly independent solutions are $f_e(z) = f_1(cz)$ and $f_o(z) = f_2(cz)/c$. In particular (the $\pm$ below corresponds to $c^2 = +i$ or $-i$ respectively and both produce the same result).

$$\begin{aligned} f_e(z) =& e^{\mp i\frac{z^2}{4}} M\left(\nu + 1/2, 2\nu + 1, 2i\left(\pm z^2/4\right)\right) \\ =& e^{\mp i\frac{z^2}{4}} \Gamma(1+\nu) e^{\pm i\frac{z^2}{4}} \left(\pm(z^2/4)/2\right)^{-\nu} J_\nu\left(\pm z^2/4\right) \\ =& \Gamma(1+\nu)\left(\pm(z^2/4)/2\right)^{-\nu} J_\nu\left(\pm z^2/4\right) \\ =& \Gamma(1+\nu)\hat{J}_\nu\left(z^2/4\right). \end{aligned} \tag{69}$$

In the second equality above, we have used the formula 13.6.1 from [42] (pg. 509) by setting $\mu = \nu$, namely

$$M\left(\mu + 1/2, 2\mu + 1, 2iz\right) = \Gamma(\mu+1) e^{iz} (z/2)^{-\mu} J_\mu(z).$$

Similarly, using the same formula with $\mu = -\nu$ gives

$$\begin{aligned} f_o(z) =& z e^{\mp i\frac{z^2}{4}} M\left(-\nu + 1/2, -2\nu + 1, 2i\left(\pm z^2/4\right)\right) \\ =& z e^{\mp i\frac{z^2}{4}} \Gamma(1-\nu) e^{\pm i\frac{z^2}{4}} \left(\pm(z^2/4)/2\right)^{\nu} J_{-\nu}\left(\pm z^2/4\right) \\ =& \Gamma(1-\nu) z \hat{J}_{-\nu}\left(z^2/4\right). \end{aligned} \tag{70}$$

A.3. The homogeneous problem

In this section, we show the inhomogeneous Eq. (29) subject to $\tilde{u}(x, y = \pm 1) = 0$ does not have unique solution unless the form (31) is assumed. This is done by showing the following homogeneous problem has a non-trivial solution

$$\left.\begin{aligned} u_{yy} + 4\omega y u_{yx} + 2\omega u_x + 8\omega^2 y^2 u_{xx} = 0, \\ u(x, y = \pm 1) = 0, \end{aligned}\right\} \tag{71}$$

where ω is a negative constant. We shall only be interested in solutions that are analytic functions in both y and x, and vanishes as $x \to \infty$. First we look for a solution of the form $u = \sum_{n=0}^{\infty} b_{2n}(x) y^{2n}$. Inserting the power series into (71) gives the recursive relation $b_2 + \omega D b_0 = 0$ and $(2n+4)(2n+3)b_{2n+4} + (4n+5)2\omega D b_{2n+2} + 2(2\omega)^2 D^2 b_{2n} = 0$ for $n \geq 0$, where $D = d/dx$. After writing out a few terms, it is evident that this leads to

$$b_{2n} = a_{2n}(2\omega)^n D^n b_0, \quad a_0 = 1, \quad a_2 = -1/2, \quad \cdots$$

As a result, the recursive relation becomes for $n \geq 0$

$$\left\{(2n+4)(2n+3)a_{2n+4} + (4n+5)a_{2n+2} + 2a_{2n}\right\} D^{n+2} b_0 = 0$$

Notice $b_0(x)$ cannot be a polynomial in order for $u \to 0$ as $x \to \infty$, thus it must be that for $n \geq 0$

$$(2n+4)(2n+3)a_{2n+4} + (4n+5)a_{2n+2} + 2a_{2n} = 0$$

To solve for a_{2n}, it is easier to convert above recursive relation back into a differential equation. This is done by multiplying the equation with z^{2n} for some auxiliary variable z and summing over $n \geq 0$. After some manipulations, we arrive at

$$\begin{aligned} &\sum_{n=1}^{\infty} 2n(2n-1)a_{2n} z^{2n-2} \cdots \\ &+ 2\sum_{n=1}^{\infty} 2n a_{2n} z^{2n} + (2z^2+1)\sum_{n=0}^{\infty} a_{2n} z^{2n} = 0. \end{aligned}$$

Setting $f = \sum_{n=0}^{\infty} a_{2n} z^{2n}$ so that above is equivalent to $f_{zz} + 2z f_z + (2z^2 + 1)f = 0$. This can be converted into an equation the form (68) by the substitution $f = \hat{f}(z) exp(-z^2/2)$ and change of variable $z \mapsto \sqrt{2}z$, thus the even solution is simply given by (69) (recall $\nu = -1/4$). Reversing the substitutions gives

$$f = e^{-z^2/2} \hat{J}_{-1/4}(z^2/2). \tag{72}$$

Recall $u = \sum_{n=0} a_{2n}(2\omega y^2)^n D^n b_0(x)$, thus the remaining is to find $b_0(x)$ such that

$$\sum_{n=0} a_{2n}(2\omega)^n D^n b_0(x) = 0. \tag{73}$$

Since a_{2n} is the power series coefficients of (72), $b_0 = exp(\alpha_j x/\omega)$ satisfies (73), where α_j is the jth positive zero of $J_{-1/4}$. As a result, $u = u_e^j$ solves (71) for all j, where

$$u_e^j = e^{\alpha_j(x/\omega - y^2)} \hat{J}_{-1/4}(\alpha_j y^2). \tag{74}$$

By starting with an odd power series in y, another set solutions can be recovered, namely $u_o^j = exp(\beta_j(x/\omega - y^2)) y \hat{J}_{1/4}\left(\beta_j y^2\right)$, where β_j is the jth positive zero of $J_{1/4}$. In fact, the set $\{u_e^j, u_o^j\}_{j=1}$ form a basis for the solutions of (71) over the space of analytic functions in y and x (up to exponential order) [43,44].

A.4. Proofs of claims in Section 6.3

$\mathcal{F}$ given by (52) can be written as $\mathcal{F}(\hat{\mu}) = s(\hat{\mu} + M)(\hat{\mu} + x) - (\hat{\mu} + y)z\hat{\mu}$. By (48)

$$\left.\begin{aligned} &\mathcal{F}(-M) > 0, \qquad \mathcal{F}(-x) > 0, \\ &\left\{\mathcal{F}(\hat{k} - M) \geq 0\right\} = \left\{\beta \geq \varsigma_5\right\}, \end{aligned}\right\} \tag{75}$$

where

$$\varsigma_5 = \varsigma_0 + \frac{z}{\hat{k}^3}\frac{\hat{k} - M}{\hat{k}}\frac{y + \hat{k} - M}{x + \hat{k} - M}.$$

Similarly, it can be shown

$$\left.\begin{aligned} \left\{f_1 - 2f_2 M \leq 0\right\} &= \left\{\varsigma_6 \leq \beta\right\}, \\ \left\{f_1 + 2f_2(\hat{k} - M) \geq 0\right\} &= \left\{\varsigma_7 \leq \beta\right\}, \\ \left\{f_1 - 2f_2 x \geq 0\right\} &= \left\{\varsigma_8 \leq \beta\right\} \end{aligned}\right\} \tag{76}$$

where

$$\left.\begin{aligned} \varsigma_6 = \varsigma_0 + \tfrac{z}{\hat{k}^3}\tfrac{y-2M}{x-M}, \qquad \varsigma_7 = \varsigma_0 + \tfrac{z}{\hat{k}^3}\tfrac{y+2(\hat{k}-M)}{x+(2\hat{k}-M)}, \\ \varsigma_8 = \varsigma_0 - \tfrac{z}{\hat{k}^3}\tfrac{y-2x}{x-M}. \end{aligned}\right\}$$

It can be shown by definitions and (48) that $(\{\varsigma_j\}_{j=0}^4$ as in (56))

$$\left.\begin{aligned} &\varsigma_4 > \varsigma_8 > \varsigma_3 > \varsigma_0 > \varsigma_2 > \varsigma_6, \\ &\varsigma_8 > \varsigma_7 > \varsigma_2, \quad \varsigma_4 > \varsigma_5, \quad \varsigma_4 > \varsigma_1 > \varsigma_2. \end{aligned}\right\} \tag{77}$$

Claim 3: $\hat{\mu}_2 \in [-M, -M + \hat{k})$ if and only if $\{\beta \geq \varsigma_4\} \cup \{\max\{\varsigma_5, \varsigma_7\} < \beta \leq \varsigma_3\}$.

Proof. It is shown in Claim 5 below that $\hat{\mu}_2 < -M$ over the region $\beta < \varsigma_2$, which is equivalent to $f_2 < 0$. As a result, it suffices to consider $f_2 > 0$. From the first half of the proof of Claim 4 below, we have $-M < \hat{\mu}_1$ whenever $f_2 > 0$ and $\Delta \geq 0$. Notice $f_2 > 0$ and $\Delta \geq 0$ implies $\hat{\mu}_1 \leq \hat{\mu}_2$, thus $\{f_2 > 0\} \cap \{\Delta \geq 0\} \subset \{-M \leq \hat{\mu}_2\}$. In other words

$$\begin{aligned}
&\{-M \leq \hat{\mu}_2\} \cap \{f_2 > 0\} \cap \{\Delta \geq 0\} \\
=&\{f_2 > 0\} \cap \{\Delta \geq 0\} \\
=&\{\beta \geq \varsigma_4\} \cup \{\varsigma_2 < \beta \leq \varsigma_3\} \qquad (78)
\end{aligned}$$

On the other hand

$$\begin{aligned}
&\{\hat{\mu}_2 < \hat{k} - M\} \cap \{f_2 > 0\} \cap \{\Delta \geq 0\} \\
=&\left\{\sqrt{\Delta} < f_1 + 2f_2(\hat{k} - M)\right\} \cap \{f_2 > 0\} \cap \{\Delta \geq 0\} \\
=&\{\mathcal{F}(\hat{k} - M) > 0\} \cap \{f_1 + 2f_2(\hat{k} - M) > 0\} \cdots \\
&\qquad \cap \{f_2 > 0\} \cap \{\Delta \geq 0\} \\
=&\{\beta > \varsigma_5\} \cap \{\beta > \varsigma_7\} \cap \{\beta > \varsigma_2\} \cdots \\
&\qquad \cap \{\{\beta \geq \varsigma_4\} \cup \{\beta \leq \varsigma_3\}\} \\
=&\{\beta \geq \varsigma_4\} \cup \{\max\{\varsigma_5, \varsigma_7\} < \beta \leq \varsigma_3\}, \qquad (79)
\end{aligned}$$

where $(75)_3$, $(76)_2$ and (78) are used for the third equality, and (77) for the fourth. Since $\varsigma_2 < \max\{\varsigma_5, \varsigma_7\}$ by (77), the claim follows by taking the intersection of (78) and (79). ■

Claim 4: $\hat{\mu}_1 \in [-M, -M + \hat{k})$ if and only if

$$\begin{aligned}
&\{\varsigma_4 \leq \beta\} \cup \{\varsigma_7 \leq \beta \leq \varsigma_3\} \cdots \\
&\cup \{\varsigma_2 < \beta < \min\{\varsigma_7, \varsigma_5, \varsigma_3\}\} \cup \{\beta < \min\{\varsigma_5, \varsigma_2\}\}.
\end{aligned}$$

Proof. First consider $f_2 = 0$, which implies $\hat{\mu}_1 = -f_0/f_1 = sxM/(yz - s(x + M))$. Since $f_2 = 0 \Leftrightarrow s = z$, it must be $\hat{\mu}_1 = -xM/(M + x - y)$, which is greater than $-M$ by (48). Now consider $f_2 < 0$. By (75), it must be that $\hat{\mu}_1$ and $\hat{\mu}_2$ are distinct real and $-M$ is strictly in between $\hat{\mu}_2$ and $\hat{\mu}_1$. By Claim 5 below, $\hat{\mu}_2 < -M$ when $f_2 < 0$. Thus it must be $-M < \hat{\mu}_1$ when $f_2 < 0$. At last, consider

$$\begin{aligned}
&\{\hat{\mu}_1 \leq -M\} \cap \{f_2 > 0\} \cap \{\Delta \geq 0\} \\
=&\left\{-(f_1 - 2f_2M) \leq \sqrt{\Delta}\right\} \cap \{f_2 > 0\} \cap \{\Delta \geq 0\}.
\end{aligned}$$

Consider the subset

$$\begin{aligned}
&\left\{-(f_1 - 2f_2M) \leq \sqrt{\Delta}\right\} \cap \{f_2 > 0\} \cap \{\Delta \geq 0\} \cdots \\
&\qquad \cap \{-(f_1 - 2f_2M) \leq 0\} \\
=&\{f_1 - 2f_2M \geq 0\} \cap \{f_2 > 0\} \cap \{\Delta \geq 0\} \\
=&\{\beta \leq \varsigma_6\} \cap \{\{\beta \geq \varsigma_4\} \cup \{\varsigma_2 < \beta \leq \varsigma_3\}\} = \emptyset,
\end{aligned}$$

where $(76)_1$ and (78) are used to obtain the second equality, and (77) for the third. Similarly

$$\begin{aligned}
&\left\{-(f_1 - 2f_2M) \leq \sqrt{\Delta}\right\} \cap \{f_2 > 0\} \cap \{\Delta \geq 0\} \cdots \\
&\qquad \cap \{-(f_1 - 2f_2M) > 0\} \\
=&\{\mathcal{F}(-M) \leq 0\} \cap \{f_2 > 0\} \cap \{\Delta \geq 0\} \cap \{f_1 - 2f_2M < 0\} \\
=&\emptyset,
\end{aligned}$$

where $(75)_1$ is used for the second equality. Since $\hat{\mu}_1 \leq -M$ is an empty set when $\Delta \geq 0$ and $f_2 > 0$, it must be $-M < \hat{\mu}_1$ when $\Delta \geq 0$ and $f_2 > 0$. In summary, $-M < \mu_1$ whenever real. Now consider the set

$$\begin{aligned}
&\{\hat{\mu}_1 < \hat{k} - M\} \cap \{f_2 > 0\} \cap \{\Delta \geq 0\} \\
=&\left\{-\sqrt{\Delta} < f_1 + 2f_2(\hat{k} - M)\right\} \cap \{f_2 > 0\} \cap \{\Delta \geq 0\}.
\end{aligned}$$

Consider the subset

$$\begin{aligned}
&\left\{-\sqrt{\Delta} < f_1 + 2f_2(\hat{k} - M)\right\} \cap \{f_2 > 0\} \cap \{\Delta \geq 0\} \cdots \\
&\qquad \cap \{f_1 + 2f_2(\hat{k} - M) \geq 0\} \\
=&\{f_1 + 2f_2(\hat{k} - M) \geq 0\} \cap \{f_2 > 0\} \cap \{\Delta \geq 0\} \\
=&\{\varsigma_7 \leq \beta\} \cap \{\varsigma_2 < \beta\} \cap \{\{\varsigma_4 \leq \beta\} \cup \{\beta \leq \varsigma_3\}\} \\
=&\{\beta \geq \varsigma_4\} \cup \{\varsigma_7 \leq \beta \leq \varsigma_3\}.
\end{aligned}$$

Similarly

$$\begin{aligned}
&\left\{-\sqrt{\Delta} < f_1 + 2f_2(\hat{k} - M)\right\} \cap \{f_2 > 0\} \cap \{\Delta \geq 0\} \cdots \\
&\qquad \cap \{f_1 + 2f_2(\hat{k} - M) < 0\} \\
=&\{\mathcal{F}(\hat{k} - M) < 0\} \cap \{\beta < \varsigma_7\} \cap \{\varsigma_2 < \beta\} \cdots \\
&\qquad \cap \{\{\varsigma_4 \leq \beta\} \cup \{\beta \leq \varsigma_3\}\} \\
=&\{\beta < \varsigma_5\} \cap \{\beta < \varsigma_7\} \cap \{\varsigma_2 < \beta\} \cap \{\{\varsigma_4 \leq \beta\} \cup \{\beta \leq \varsigma_3\}\} \\
=&\{\varsigma_2 < \beta < \min\{\varsigma_7, \varsigma_5, \varsigma_3\}\}.
\end{aligned}$$

In addition

$$\begin{aligned}
&\{\hat{\mu}_1 < \hat{k} - M\} \cap \{f_2 < 0\} \cap \{\Delta \geq 0\} \\
=&\left\{\sqrt{\Delta} < -(f_1 + 2f_2(\hat{k} - M))\right\} \cap \{f_1 + 2f_2(\hat{k} - M) < 0\} \cdots \\
&\qquad \cap \{f_2 < 0\} \cap \{\Delta \geq 0\} \\
=&\{\mathcal{F}(\hat{k} - M) < 0\} \cap \{f_1 + 2f_2(\hat{k} - M) < 0\} \cdots \\
&\qquad \cap \{f_2 < 0\} \cap \{\Delta \geq 0\} \\
=&\{\beta < \varsigma_5\} \cap \{\beta < \varsigma_7\} \cap \{\beta < \varsigma_2\} \cap \{\{\varsigma_4 \leq \beta\} \cup \{\beta \leq \varsigma_3\}\} \\
=&\{\beta < \varsigma_5\} \cap \{\beta < \varsigma_7\} \cap \{\beta < \varsigma_2\} \cap \{\beta \leq \varsigma_3\} \\
=&\{\beta < \min\{\varsigma_5, \varsigma_2\}\}.
\end{aligned}$$

Taking union of the last three sets yields the result. ■

Claim 5: $\{\hat{\mu}_2 < -M\} = \{\beta < \varsigma_2\}$.

Proof. In particular

$$\begin{aligned}
&\{\hat{\mu}_2 < -M\} \cap \{f_2 > 0\} \cap \{\Delta \geq 0\} \\
=&\left\{\sqrt{\Delta} < f_1 - 2f_2M\right\} \cap \{f_2 > 0\} \cap \{\Delta \geq 0\} \\
=&\left\{\sqrt{\Delta} < f_1 - 2f_2M\right\} \cap \{0 < f_1 - 2f_2M\} \cdots \\
&\qquad \cap \{f_2 > 0\} \cap \{\Delta \geq 0\} \\
=&\{0 < \mathcal{F}(-M)\} \cap \{0 < f_1 - 2f_2M\} \cap \{f_2 > 0\} \cap \{\Delta \geq 0\} \\
=&\{0 < f_1 - 2f_2M\} \cap \{f_2 > 0\} \cap \{\Delta \geq 0\} \\
=&\{\beta < \varsigma_6\} \cap \{\varsigma_2 < \beta\} \cap \{\Delta \geq 0\} = \emptyset, \qquad (80)
\end{aligned}$$

where last equality is because $\varsigma_6 < \varsigma_2$ by $(77)_1$. On the other hand

$$\begin{aligned}
&\{\hat{\mu}_2 < -M\} \cap \{\Delta \geq 0\} \cap \{f_2 < 0\} \\
=&\left\{\sqrt{\Delta} > f_1 - 2f_2M\right\} \cap \{\Delta \geq 0\} \cap \{f_2 < 0\}.
\end{aligned}$$

Consider the subset of above

$$\begin{aligned}
&\left\{\sqrt{\Delta} > f_1 - 2f_2M\right\} \cap \{\Delta \geq 0\} \cap \{f_2 < 0\} \cdots \\
&\qquad \cap \{f_1 - 2f_2M > 0\} \\
=&\{\mathcal{F}(-M) > 0\} \cap \{\Delta \geq 0\} \cap \{f_2 < 0\} \cdots \\
&\qquad \cap \{f_1 - 2f_2M > 0\} \\
=&\{\beta < \varsigma_6\} \cap \{\Delta \geq 0\} \cap \{\beta < \varsigma_2\} = \{\beta < \varsigma_6\}. \qquad (81)
\end{aligned}$$

Similarly

$$\begin{aligned}
&\left\{\sqrt{\Delta} > f_1 - 2f_2M\right\} \cap \{\Delta \geq 0\} \cap \{f_2 < 0\} \cdots \\
&\qquad \cap \{f_1 - 2f_2M \leq 0\} \\
=&\{f_1 - 2f_2M \leq 0\} \cap \{\Delta \geq 0\} \cap \{f_2 < 0\} \\
=&\{\varsigma_6 \leq \beta\} \cap \{\Delta \geq 0\} \cap \{\beta < \varsigma_2\} \\
=&\{\varsigma_6 \leq \beta < \varsigma_2\}. \qquad (82)
\end{aligned}$$

Taking the union of (80), (81) and (82), the claim follows. ■

Claim 6: $\partial\Re\{\hat{\mu}_2\}/\partial\beta < 0$ if and only if $\{\beta \le \varsigma_4\} \cap \{\beta \ne \varsigma_2\}$.

Proof. If $\Delta \le 0$, then $\Re\{\hat{\mu}_2\} := -f_1/(2f_2)$. By definition (53)

$$\partial\Re\{\hat{\mu}_2\}/\partial\beta = \hat{k}^3 z\,(x+M-y)\,/(2f_2^2),$$

which is negative by (48). As a result

$$\begin{aligned}&\{\partial\Re\{\hat{\mu}_2\}/\partial\beta < 0\} \cap \{\Delta \le 0\}\\ =&\{\Delta \le 0\} \overset{(55)_2}{=} \{\varsigma_3 \le \beta \le \varsigma_4\}.\end{aligned} \tag{83}$$

If $\Delta > 0$, taking implicit differentiation with respect to β of $f_2\hat{\mu}_2^2 + f_1\hat{\mu}_2 + f_0 = 0$ gives $(\partial f_2/\partial\beta)\hat{\mu}_2^2 + (\partial f_1/\partial\beta)\hat{\mu}_2 + (\partial f_0/\partial\beta) + (2f_2\hat{\mu}_2 + f_1)(\partial\hat{\mu}_2/\partial\beta) = 0$. Substituting (53) and $2f_2\hat{\mu}_2 + f_1 := \sqrt{\Delta}$ gives $\partial\hat{\mu}_2/\partial\beta = -\hat{k}^3\left(\hat{\mu}_2 + x\right)\left(\hat{\mu}_2 + M\right)/\sqrt{\Delta}$. By (48), $\partial\hat{\mu}_2/\partial\beta < 0$ (provided $\Delta > 0$) if and only if $\hat{\mu}_2 < -M$ or $\hat{\mu}_2 > -x$. Notice $\{f_2 < 0\} = \{\hat{\mu}_2 < -M\}$ by $(55)_1$ and Claim 5, thus

$$\begin{aligned}&\left\{\left\{\hat{\mu}_2 < -M\right\} \cup \left\{\hat{\mu}_2 > -x\right\}\right\} \cap \left\{f_2 < 0\right\} \cap \{\Delta > 0\}\\ =&\left\{\beta < \varsigma_2\right\}\end{aligned} \tag{84}$$

On the other hand

$$\begin{aligned}&\left\{\left\{\hat{\mu}_2 < -M\right\} \cup \left\{\hat{\mu}_2 > -x\right\}\right\} \cap \left\{f_2 > 0\right\} \cap \{\Delta > 0\}\\ =&\left\{\hat{\mu}_2 > -x\right\} \cap \left\{f_2 > 0\right\} \cap \{\Delta > 0\}\\ =&\left\{\sqrt{\Delta} > f_1 - 2f_2x\right\} \cap \left\{f_2 > 0\right\} \cap \{\Delta > 0\}.\end{aligned}$$

Consider the subset

$$\begin{aligned}&\left\{\sqrt{\Delta} > f_1 - 2f_2x\right\} \cap \left\{f_2 > 0\right\} \cap \{\Delta > 0\} \cdots\\ &\qquad \cap \left\{f_1 - 2f_2x \ge 0\right\}\\ =&\{\mathcal{F}(-x) < 0\} \cap \left\{f_2 > 0\right\} \cap \{\Delta > 0\} \cap \left\{f_1 - 2f_2x \ge 0\right\}\\ =&\emptyset,\end{aligned}$$

where $(75)_2$ is used for the second equality. In addition

$$\begin{aligned}&\left\{\sqrt{\Delta} > f_1 - 2f_2x\right\} \cap \left\{f_2 > 0\right\} \cap \{\Delta > 0\} \cdots\\ &\qquad \cap \left\{f_1 - 2f_2x < 0\right\}\\ =&\left\{f_1 - 2f_2x < 0\right\} \cap \left\{f_2 > 0\right\} \cap \{\Delta > 0\}\\ =&\left\{\varsigma_2 < \beta < \varsigma_8\right\} \cap \{\Delta > 0\} = \left\{\varsigma_2 < \beta < \min\{\varsigma_3, \varsigma_8\}\right\}\\ =&\left\{\varsigma_2 < \beta < \varsigma_3\right\},\end{aligned} \tag{85}$$

where last two equalities are due to (77). As a result, taking (83)∪(84)∪(85) yields the claim. ■

A.5. Proof for Section 6.4

Claim: Let $\mathcal{F}(\hat{\mu})$ be as in (45) and $\{f_j\}_{j=0}^3$ as in (46), then

1. one root of $\mathcal{F}(\hat{\mu})$ is negative real and bounded above by $-M$.
2. the real part of the other two roots are bounded below by $-M$.

Proof. The first part is equivalent to the statement that one of the roots of $\hat{F}(\xi) \overset{def}{=} \mathcal{F}(\xi - M)$ is negative real, and the second part is equivalent to the statement that other two roots of $\hat{F}(\xi)$ have positive real parts. After expansion and some regrouping, we have $\hat{F}(\xi) = \hat{f}_3\xi^3 + \hat{f}_2\xi^2 + \hat{f}_1\xi + \hat{f}_0$, where (recall from $(46)_1$ that $0 < f_3 < 3$ by definition)

$$\left.\begin{aligned}\hat{f}_3 &= f_3,\\ \hat{f}_2 &= s - Mf_3 + (f_3/3 - 1)z + f_3(x - M),\\ \hat{f}_1 &= (2M - y)(1 - f_3/3)z + (Mf_3 - s)(M - x),\\ \hat{f}_0 &= (1 - f_3/3)M(y - M)z.\end{aligned}\right\}$$

Since $\hat{F}$ is a cubic polynomial with real coefficients, the first part of the claim follows directly from $\hat{f}_3 > 0$ and $\hat{F}(0) := \hat{f}_0 > 0$ (by (48)). Wlog, we denote ξ_1 to be the root of $\hat{F}$ satisfying $\xi_1 < 0$, and ξ_2, ξ_3 to be the remaining two roots. For the second part of the claim, we need to show $0 < \Re\{\xi_2\}, \Re\{\xi_3\}$. Eliminating the term $Mf_3 - s$ in $\hat{f}_1$ by using $\hat{f}_2$ gives $\hat{f}_1 = (M - y + x)(1 - f_3/3)z - f_3(M - x)^2 - \hat{f}_2(M - x)$. By (48), $\hat{f}_1 < 0$ if $\hat{f}_2 > 0$. Since $\hat{f}_3 > 0$ and $\xi_1 < 0$, Routh–Hurwitz criterion states $\Re\{\xi_2\}, \Re\{\xi_3\} < 0$ if and only if (a) $\hat{f}_2 > 0$ and (b) $\hat{f}_2\hat{f}_1 > \hat{f}_0\hat{f}_3$. However, (a) and (b) cannot hold simultaneously because, if (a) holds, then the l.h.s of (b) is negative (since $\hat{f}_2 > 0$ implies $\hat{f}_1 < 0$) whereas the r.h.s of (b) is positive. In other words, at least one of $\Re\{\xi_2\}$ or $\Re\{\xi_3\}$ must be non-negative. Since $\xi_2, \xi_3 \ne 0$ (as $\hat{F}(0) > 0$), there are four possible configurations, namely (i) ξ_2 and ξ_3 are positive real, or (ii) ξ_2 and ξ_3 are non-real complex conjugates with positive real parts, or (iii) ξ_2 and ξ_3 are purely imaginary complex conjugates, or (iv) one of ξ_2 or ξ_3 is positive real and the other one is negative. To complete the proof, we show (iii) and (iv) cannot happen. Suppose (iii) is true, then $\xi_1 = -\hat{f}_2/\hat{f}_3$ and $\xi_2\xi_3 = |\xi_2|^2 = \hat{f}_1/\hat{f}_3$ by Vieta's formulas, which in turn implies $\hat{f}_2 > 0$ and $\hat{f}_1 > 0$ because $\xi_1 < 0$ and $\hat{f}_3 > 0$. This is a contradiction because $\hat{f}_2 > 0$ implies $\hat{f}_1 < 0$. Suppose (iv) is true, i.e. two negative roots and one positive root. Since $\hat{f}_3 > 0$, it must be $\hat{F} < 0$ in between its two right most roots, between which there contains 0. But $\hat{F}(0) > 0$, a contradiction. ■

A.6. Remark for Section 6.2

To put (50) back into dimensional form, recall that the dimensionless growth rate μ and wavenumber k relate to their dimensional counterparts (superscript '$*$') through $\mu^* t^* = \mu t$ and $k^* z^* = kz$. Since $t^* = tL/V$ and $z^* = Lz$, we have $\mu = \mu^* T$ and $k = Lk^*$. The dimensional basic velocity (averaged) $\langle U^*\rangle$ relates to $\langle U\rangle$ through $\langle U^*\rangle = V\langle U\rangle$. By (8) and $(9)_3$, $Ca^{-1} = \gamma b^2/(VL^2(\eta^- + \eta^+))$. By (7), $[\![R_\eta]\!] = R_\eta^r - R_\eta^l = (\eta^+ - \eta^-)/(\eta^- + \eta^+)$. Using such relations, the dimensional form of (50) reads

$$\mu^{*,st} = -\frac{b^2}{3}\frac{\gamma}{\eta^- + \eta^+}(k^*)^3 + \frac{\eta^+ - \eta^-}{\eta^- + \eta^+}\langle U^*\rangle k^*.$$

References

[1] P.G. Saffman, G. Taylor, Penetration of a fluid into a porous medium or Hele-Shaw cell containing a more viscous liquid, Proc. R. Soc. A Math. Phys. Eng. Sci. 245 (1958) 312–329, http://dx.doi.org/10.1098/rspa.1958.0085, 06.

[2] R.L. Chouke, P. van Meurs, C. van der Poel, The instability of slow, immiscible, viscous liquid-liquid displacements in permeable media, Trans. AIME 216 (1959) 188–194, http://dx.doi.org/10.2118/1141-G.

[3] S. Hill, Channeling in packed columns, Chem. Eng. Sci. 1 (1952) 247–253, http://dx.doi.org/10.1016/0009-2509(52)87017-4.

[4] G. Homsy, Viscous fingering in porous media, Annu. Rev. Fluid Mech. 19 (1987) 271–311, http://dx.doi.org/10.1146/annurev.fl.19.010187.001415.

[5] D.A. Reinelt, Interface conditions for two-phase displacement in Hele-Shaw cells, J. Fluid Mech. 183 (1987) 219–234, http://dx.doi.org/10.1017/S0022112087002611.

[6] P. Saffman, Viscous fingering in Hele-Shaw cells, J. Fluid Mech. 173 (1986) 12, http://dx.doi.org/10.1017/S0022112086001088.

[7] C. Park, G. Homsy, Two-phase displacement in Hele Shaw cells: Theory, J. Fluid Mech. 139 (1984) 291–308, http://dx.doi.org/10.1017/S0022112084000367, 02.

[8] J. Nittmann, G. Daccord, H. Stanley, Fractal growth of viscous fingers: quantitative characterization of a fluid instability phenomenon, Nature 314 (1985) 141–144, http://dx.doi.org/10.1038/314141a0, 03.

[9] G. Daccord, J. Nittmann, H. Stanley, Radial viscous fingers and diffusion-limited aggregation: Fractal dimension and growth sites, Phys. Rev. Lett. 56 (1986) 336–339, http://dx.doi.org/10.1103/PhysRevLett.56.336, 02.

[10] E. Lemaire, P. Levitz, G. Daccord, H. Van Damme, From viscous fingering to viscoelastic fracturing in colloidal fluids, Phys. Rev. Lett. 67 (1991) 2009–2012, http://dx.doi.org/10.1103/PhysRevLett.67.2009, 11.

[11] K. McCloud, J. Maher, Experimental perturbations to Saffman–Taylor flow, Phys. Rep. 260 (1995) 139–185, http://dx.doi.org/10.1016/0370-1573(95)91133-U, 09.

[12] A. Buka, J. Kertesz, T. Vicsek, Transitions of viscous fingering patterns in nematic liquid crystals, Nature 323 (1986) 424–425, http://dx.doi.org/10.1038/323424a0.

[13] A. Buka, P. Palffy-Muhoray, Morphological phase transitions in viscous fingering patterns in the liquid crystal, J. Phys. France 49 (1988) 1319–1323, http://dx.doi.org/10.1051/jphys:019880049080131900.

[14] H. Zhao, J.V. Maher, Associating-polymer effects in a Hele-Shaw experiment, Phys. Rev. E. 47 (1993) 4278–4283, http://dx.doi.org/10.1103/PhysRevE.47.4278.
[15] H. Van Damme, E. Lemaire, Y. Ould, Y. Mohamed Abdelhaye, A. Mourchid, P. Levitz, Pattern Formation in Particulate Complex Fluids: A Guided Tour, Vol. 437, Springer, 1994, pp. 134–150, http://dx.doi.org/10.1007/3-540-58652-0_34.
[16] A. Lindner, D. Bonn, J. Meunier, Viscous fingering in complex fluids, J. Phys.: Condens. Matter 12 (2000a) A477, http://dx.doi.org/10.1088/0953-8984/12/8A/366, 02.
[17] E. Poire, M. Ben Amar, Finger behavior of a shear thinning fluid in a Hele-Shaw cell, Phys. Rev. Lett. 81 (1998) 07, http://dx.doi.org/10.1103/PhysRevLett.81.2048.
[18] A. Lindner, D. Bonn, J. Meunier, Viscous fingering in a shear-thinning fluid, Phys. Fluids 12 (2000b) 256–261, http://dx.doi.org/10.1063/1.870303, 02.
[19] D. Bonn, H. Kellay, M. Ben Amar, J. Meunier, Viscous finger widening with surfactants and polymers, Phys. Rev. Lett. 75 (1995) 2132–2135, http://dx.doi.org/10.1103/PhysRevLett.75.2132, 10.
[20] S. Wilson, The Taylor-Saffman problem for a non-Newtonian liquid, J. Fluid Mech. 220 (1990) 413–425, http://dx.doi.org/10.1017/S0022112090003329, 11.
[21] J. Sader, D. Chan, B. Hughes, Non-Newtonian effects on immiscible viscous fingering in a radial Hele-Shaw cell, Phys. Rev. E 49 (1994) 420–432, http://dx.doi.org/10.1103/PhysRevE.49.420, 02.
[22] L. Kondic, M. Shelley, P. Palffy-Muhoray, Non-Newtonian Hele-Shaw flow and the Saffman–Taylor instability, Phys. Rev. Lett. 80 (1998) 02, http://dx.doi.org/10.1103/PhysRevLett.80.1433.
[23] L. Kondic, P. Palffy-Muhoray, M. Shelley, Models of non-Newtonian Hele-Shaw flow, Phys. Rev. E 54 (1996) R4536–R4539, http://dx.doi.org/10.1103/PhysRevE.54.R4536, 12.
[24] M. Ben Amar, E. Poire, Pushing a non-Newtonian fluid in a Hele-Shaw cell: From fingers to needles, Phys. Fluids 11 (1999) 1757–1767, http://dx.doi.org/10.1063/1.870041, 07.
[25] S. Mora, M. Manna, Saffman–Taylor instability for generalized Newtonian fluids, Phys. Rev. E 80 (2009) 016308, http://dx.doi.org/10.1103/PhysRevE.80.016308, 08.
[26] P. Fast, L. Kondic, M. Shelley, P. Palffy-Muhoray, Pattern formation in non-Newtonian Hele-Shaw flow, Phys. Fluids 13 (2001) 1191–1212, http://dx.doi.org/10.1063/1.1359417, 05.
[27] J. Fontana, E. Dias, J. Miranda, Controlling and minimizing fingering instabilities in non-Newtonian fluids, Phys. Rev. E 89 (2014) 01, http://dx.doi.org/10.1103/PhysRevE.89.013016.
[28] A. Lindner, P. Coussot, D. Bonn, Viscous fingering in a yield stress fluid, Phys. Rev. Lett. 85 (2000c) 314–317, http://dx.doi.org/10.1103/PhysRevLett.85.314, 08.
[29] A. Lindner, D. Bonn, E. Poire, M. Ben Amar, J. Meunier, Viscous fingering in non-Newtonian fluids, J. Fluid Mech. 469 (2002) 237–256, http://dx.doi.org/10.1017/S0022112002001714, 10.
[30] J. Nase, A. Lindner, C. Creton, Pattern formation during deformation of a confined viscoelastic layer: From a viscous liquid to a soft elastic solid, Phys. Rev. Lett. 101 (2008) 074503, http://dx.doi.org/10.1103/PhysRevLett.101.074503, 09.
[31] B. Saintyves, O. Dauchot, E. Bouchaud, Bulk elastic fingering instability in Hele-Shaw cells, Phys. Rev. Lett. 111 (2012) 06, http://dx.doi.org/10.1103/PhysRevLett.111.047801.
[32] S. Mora, M. Manna, From viscous fingering to elastic instabilities, J. Non-Newton. Fluid Mech. 173–174 (2012) 30–39, http://dx.doi.org/10.1016/j.jnnfm.2012.01.010, 04.
[33] J. Oldroyd, On the formulation of rheological equations of state, Proc. R. Soc. Lond. Ser. A Math. Phys. Eng. Sci. 200 (1950) 523–541, http://dx.doi.org/10.1098/rspa.1950.0035, 02.
[34] P. Daripa, Saffman–Taylor instability for a non-Newtonian fluid, Bull. Amer. Phys. Soc. 58 (18) (2013) 421.
[35] P. Daripa, Instability of displacement of an Oldroyd-B fluid by air in a Hele-Shaw cell, Bull. Amer. Phys. Soc. 59 (1) (2014).
[36] J.S. Ro, G.M. Homsy, Viscoelastic free surface flows: thin film hydrodynamics of Hele-Shaw and dip coating flows, J. Non-Newton. Fluid Mech. 57 (2–3) (1995) 203–225, http://dx.doi.org/10.1016/0377-0257(94)01329-G, 05.
[37] R.B. Bird, C.F. Curtiss, R.C. Armstrong, O. Hassager, Dynamics of Polymeric Liquids, Volume 2: Kinetic Theory, Wiley, 1987.
[38] M. Renardy, Mathematical Analysis of Viscoelastic Flows, SIAM, 2000, http://dx.doi.org/10.1137/1.9780898719413.
[39] A. Morozov, S. Spagnolie, Introduction to complex fluids, in: S. Spagnolie (Ed.), Complex Fluids in Biological Systems, Springer, New York, NY, 2015, pp. 3–52, http://dx.doi.org/10.1007/978-1-4939-2065-5_1.
[40] P. Drazin, W. Reid, Hydrodynamic Stability, Cambridge University Press, 2004, http://dx.doi.org/10.1017/CBO9780511616938.
[41] G.N. Watson, A Treatise on the Theory of Bessel Functions, Univ. Pr, 1966.
[42] M. Abramowitz, I.A. Stegun, Handbook of Mathematical Functions with Formulas, Graphs, and Mathematical Tables, U.S. Dept. of Commerce, National Bureau of Standards, 1972.
[43] D.G. Dickson, Infinite order differential equations, Proc. Amer. Math. Soc. 15 (1964) 639–641, http://dx.doi.org/10.1090/S0002-9939-1964-0176182-4.
[44] D.G. Dickson, Analytic mean periodic functions, Trans. Amer. Math. Soc. 110 (1964) 361–374, http://dx.doi.org/10.1090/S0002-9947-1964-0167608-5.